

Implications of different nitrogen input sources for potential production and carbon flux estimates in the coastal Gulf of Mexico (GOM) and Korean coastal waters

Jongsun Kim,^{a*} Piers Chapman,^{a*} Gilbert Rowe^{a, b}, Steven F DiMarco^a, and Daniel Thornton^a

^a Department of Oceanography, Texas A&M University, College Station, TX 77843-3146, USA

^b Department of Marine Biology, Texas A&M University, Galveston, TX 77553, USA

* Corresponding authors

*J. Kim. Email: jongsun@tamu.edu.

*P. Chapman. Email: piers.chapman@tamu.edu.

Submit to Ocean Sciences

Abstract

The coastal Gulf of Mexico (GOM) and Coastal Sea off Korea (CSK) both suffer from human-induced eutrophication. We used a N-mass balance model in two different regions with different nitrogen input sources to estimate organic carbon fluxes and predict future carbon fluxes under different model scenarios. The coastal GOM receives nitrogen predominantly from the Mississippi and Atchafalaya Rivers and atmospheric nitrogen deposition (AN-D) is only a minor component in this region. However, in the CSK, groundwater and atmospheric nitrogen deposition are more important controlling factors. Our model includes the fluxes of nitrogen to the ocean from the atmosphere, groundwater, and rivers, based on observational and literature data, and identifies three zones (brown, green and blue waters) in the coastal GOM and CSK with different productivity and carbon fluxes. Based on our model results, the potential primary production rate in the inner (brown water) zone are more than 2 (GOM) and 1.5 gC m⁻² day⁻¹ (CSK). In the middle (green water) zone, potential production is between 0.1 to 2 (GOM) and 0.3 to 1.5 gC m⁻² day⁻¹ (CSK). In the offshore (blue water) zone, productivity is less than 0.1 (GOM) and 0.3 (CSK) gC m⁻² day⁻¹. Through our model scenario results, overall oxygen demand in the GOM would increase approximately 21% if we fail to reduce riverine N input, likely increasing considerably the area affected by hypoxia. Comparing the results from the U.S. with those from Korea shows the importance of considering both riverine and atmospheric inputs of nitrogen. This has direct implications for investigating how changes in energy technologies can lead to changes in the production of various atmospheric contaminants that affect air quality, climate and the health of local populations.

Keywords:

Chemical tracers, Biological processes, Shelf-seas, Gulf of Mexico, Yellow Sea.

1 **Introduction**

2 Industrial expansion and anthropogenic emissions are major factors leading to increased
3 coastal productivity and potential eutrophication (Sigman and Hain 2012). Coastal primary
4 production is controlled largely by nitrogen (N) and phosphorus (P), and the relative supply of
5 each determines which element limits production (Paerl 2009); freshwater inputs and the
6 distance from sources such as river mouths are also important (Dodds and Smith 2016).
7 Changes in nutrient loading from air-borne, river-borne and groundwater sources can also affect
8 which element limits coastal productivity (Sigman and Hain 2012). Most coastal regions are N-
9 limited, however, at certain times conditions can change from N-limited to P-limited (Dodds and
10 Smith 2016; Howarth and Marino 2006). Sylvan et al. (2006), for example, suggested that the
11 coastal GOM, especially near the Mississippi River delta mouth, is P-limited at certain times.

12 Several studies have shown that increasing atmospheric nitrogen deposition (AN-D) is
13 contributing to ocean production globally, including to eutrophication, and is potentially of future
14 importance in the GOM (Cornell et al., 1995; Doney et al., 2007; Duce et al., 2008; He et al.,
15 2010; Kanakidou et al., 2016; Kim 2018; Kim (TW) et al., 2011; Lawrence et al., 2000; Paerl et
16 al., 2002). Recently, Kim (TW) et al. (2011), using a model simulation showed that AN-D
17 controls approximately 52% of the coastal productivity in the Yellow Sea. Global NOx
18 emissions have increased but appear to be changing differently in the US and Asia (Kim (JY) et
19 al., 2010; Luo et al., 2014; Shou et al., 2018; Zhao et al., 2015), and may affect not only coastal
20 productivity but also global total nitrogen budgets. This study uses a box model to define
21 potential carbon fluxes based on different nitrogen input sources in two different regions, the
22 Coastal Gulf of Mexico (GOM) and the Coastal Sea off Korea (CSK). The GOM and CSK
23 were selected in this study because while the major input source to the coastal ocean in both

24 regions is riverine, the AN-D and SGD are considerably more important in the CSK region
25 (Wade and Sweet, 2008; Zhao et al., 2015).

26 Most previous model studies in the GOM have been used to predict the size of the
27 hypoxic zone (e.g., Fennel et al., 2006, 2011, 2013; Green et al., 2008; Hetland and DiMarco
28 2008; Justic et al., 2002; Scavia et al., 2004; Turner et al. 2006, 2008), although Bierman et al.
29 (1994), used a mass balance model to estimate carbon flux and oxygen exchange. The mass
30 balance model is a useful tool to calculate nutrient or carbon fluxes and to estimate production in
31 the coastal ocean (Kim (JS) et al, 2010; Kim (G) et al., 2011), and such models have been
32 successfully used in many regions and individual coastal systems to estimate ecosystem
33 metabolism, e.g., in the Patuxent River estuary of the Chesapeake Bay (Hagy et al. 2000; Testa et
34 al., 2008) and in the LOICZ (Land Ocean Interactions in the Coastal Zone) project (e.g., Ramesh
35 et al., 2015). However, there are few such model studies in the GOM and CSK. All previous
36 models for the GOM and the CSK have considered only riverine N as the predominant input
37 source, and no one has considered AN-D as an input in either region.

38 In this study, we aimed to: 1) build a mass balance model considering not only riverine N
39 input but also air-borne and groundwater-borne N; 2) use it to calculate potential primary
40 production in the three regions defined by Rowe and Chapman (2002, henceforth RC02, see next
41 section) and their associated coastal productivity; and 3) use the mass balance model to test the
42 RC02 hypothesis. Because RC02 did not quantify their model with nutrient data and no one
43 has applied this model to another region, we tested the RC02 hypothesis using data from both the
44 GOM and the CSK that include low salinity samples. We used historical data from the mid-
45 western part of the CSK and evaluated the theoretical model of RC02 in both areas where
46 freshwater with high terrestrial nutrient input mixes into the coastal ocean.

47

48 **Study areas**

49 The Texas-Louisiana (LATEX) shelf in the northern Gulf of Mexico is affected by
50 coastal nutrient loading, leading to hypoxia, coming from two major terrestrial sources (the
51 Mississippi and Atchafalaya Rivers that together form the Mississippi-Atchafalaya River System
52 MARS). These two major rivers have different nutrient concentrations. The Gulf of Mexico
53 (GOM) is a semi-enclosed oligotrophic sea and the MARS is the major source of nutrients and
54 freshwater to the northern GOM (Alexander et al., 2008; Rabalais et al., 2002; Robertson and
55 Saad, 2014). The MARS drains 41% of the contiguous United States (Milliman and Meade,
56 1983) and discharges approximately $20,000 \text{ m}^3 \text{ s}^{-1}$, or about 60% of the total freshwater flow,
57 (about $10.6 \times 10^{11} \text{ m}^3 \text{ year}^{-1}$ or $3.4 \times 10^4 \text{ m}^3 \text{ s}^{-1}$) to the northern side of the GOM. The
58 remainder comes from other U.S. rivers, Mexico and Cuba (Nipper et al., 2004).

59 At the Old River Control Structure on the lower Mississippi River approximately 25% of
60 the Mississippi River's water is diverted into the Atchafalaya River, where it mixes with the
61 water in the Red River. The flow in the Atchafalaya River totals 30% of the total MARS flow
62 (Figure 1a). Several projects have investigated the relationship between nutrients and the
63 marine ecosystem, and how this leads to hypoxia in the GOM (e.g. Bianchi et al., 2010; Diaz and
64 Rosenberg, 1995, 2008; Forrest et al., 2011; Hetland and DiMarco, 2008; Laurent et al., 2012;
65 Quigg et al., 2011; Rabalais and Smith, 1995; Rabalais et al., 2007; Rabalais and Turner 2001;
66 Rowe and Chapman 2002). Strong stratification due to the high freshwater discharge from the
67 MARS, winds and nitrate concentration all affect hypoxia formation, with upwelling-favorable
68 wind facilitating its development (Feng et al., 2012, 2014).

69 In the Northern GOM, the major factor controlling coastal productivity is riverine N input.

70 Rowe and Chapman (2002), defined three theoretical zones over the LATEX shelf close to the
71 Mississippi and Atchafalaya River mouths to predict the effects of nutrient loading on hypoxia
72 along the river plumes and over the shelf. They named these the brown, green, and blue zones
73 (Figure 2). Nearest the river mouths is a ‘brown’ zone, where the nutrient concentrations are
74 high, but the discharge of sediment from the river reduces light penetration and limits primary
75 productivity within the plume. Further away from the river plume is a stratified ‘green’ zone
76 with available light and nutrients that result in high productivity. In this region, the rapid
77 depletion of nutrients is due to biological uptake processes that depend on the season and river
78 flow (Bode and Dortch, 1996; Dortch and Whitedge, 1992; Lohrenz et al., 1999; Turner and
79 Rabalais, 1994). Still further offshore, and also along the river plume to the west, there is the
80 so-called ‘blue’ zone, defined arbitrarily by nitrate concentrations of $1 \mu\text{M L}^{-1}$ or less, which is
81 dominated by intense seasonal stratification and a strong pycnocline, so that in the surface layer
82 nutrients are limiting at this distance from the rivers and most primary production is fueled by
83 recycled nutrients (Dortch and Whitedge, 1992). It is important to note that RC02 makes clear
84 that the edges of the zones (geographical regimes) are not static, but change over time depending
85 on season, river flow, and biological processes (Figure 2).

86 The coastal sea off western Korea (CSK) forms the eastern side of another semi-enclosed
87 basin (the Yellow Sea) and is affected by freshwater discharge from river plumes in the same
88 way as the coastal GOM, although the freshwater flow is considerably less. The Yellow Sea
89 covers about 380,000 km² area with an average water depth of 44 m, and numerous islands are
90 located on its eastern side (Liu et al., 2003). Our specific study area is the mid-western coastal
91 region from the Taean Peninsula to Gomso Bay (Figures 1c and 1d).

92 There is a strong tidal front in the coastal area near the Taean Peninsula due to sea floor

93 topography and the coastal configuration (Park, 2017; Park et al., 2017). The region also
94 contains several bays (Garolim Bay, Gomso Bay and Cheonsu Bay), and is affected by
95 discharges from a large artificial lake (Saemangeum lake) as well as the freshwater discharge
96 from the Keum river plume that contains high concentrations of nutrients (Lim et al., 2008).
97 Conditions in the mid-western CSK near the Taean peninsula are similar to the coastal GOM,
98 because of mixing of two different water masses from Gyunggi Bay (Han River) and the Keum
99 River (Choi et al., 1998, 1999). The annual mean flow rates within the Keum River were about
100 $70 \text{ m}^3 \text{ s}^{-1}$ (normal period) and $170 \text{ m}^3 \text{ s}^{-1}$ (flood period) (Yang and Ahn 2008). Precipitation
101 within the catchment was $1,208 \text{ mm year}^{-1}$ during 2003 to 2005 (Yang and Ahn 2008).

102 Unlike the coastal GOM, the CSK has increased nitrogen inputs from atmospheric
103 nitrogen deposition (AN-D, which is approximately five times higher than in the GOM, Table 2)
104 (Kim (JY) et al., 2010; Luo et al., 2014; Shou et al., 2018; Zhao et al., 2015) and nutrient inputs
105 from the groundwater discharge (Kim (JS) et al., 2010; Kim (G) et al., 2011). AN-D has
106 increased in the CSK owing to industrial development in China during the last few decades,
107 which has led to increased atmospheric N emission.

108

109 **Data and Methods**

110 *Riverine N data*

111 Hydrographic data from the MCH (Mechanisms Controlling Hypoxia – MCH Atlas)
112 projects in the Gulf of Mexico were collected from the National Oceanographic Data Center
113 (<https://www.nodc.noaa.gov>) covering the period from 2004 through 2007 (Table 1). We
114 excluded cruises MCH M6 and M7 because the threat of hurricanes led to sampling stations in
115 different areas from the other cruises. The study sites and sampling areas are shown in Figure

116 1b. Quality control removed inconsistencies and anomalies in the data (e.g., removing outliers,
117 missing data interpolation). Hydrographic data from the CSK (nutrients, salinity, oxygen) were
118 collected during several cruises (Table 1 and Figure 1c and 1d), and the data were put through
119 similar QA/QC routines.

120

121 *Atmospheric Nitrogen Deposition (AN-D) data*

122 AN-D data from around the US are sparse (Table 2). Most US data have been collected
123 along the east coast of the US and the only data in the GOM region were collected near Corpus
124 Christi (~10 kg/ha/year; Wade and Sweet, 2008). Considerable AN-D could be expected,
125 however, from the large number of petrochemical and fertilizer plants in southern TX, especially
126 near Houston and along the Mississippi. While there are more data from the Yellow Sea (Kim
127 (JY) et al., 2010; Luo et al., 2014; Shou et al., 2018; Zhao et al., 2015), they are still limited
128 owing to the broad sampling coverage. While AN-D data in the Asian region were up to 140
129 kg/ha/year, data from the eastern side of the US were under 10 Kg/ha/year, even lower than in
130 the GOM, suggesting there is currently not a large contribution from AN-D to total N loads to the
131 North Atlantic Ocean. The approximate order of magnitude difference in AN-D concentrations
132 between the GOM and the CSK is due to the continuing industrial development in East Asia and
133 the resulting N emissions (Wang et al., 2016; Zhao et al., 2015). Lamarque et al., (2013)
134 reported model results, which covers our study regions, and their model appears to underestimate
135 AN-D at the sampling sites compared with observational data in the GOM (Wade and Sweet,
136 2008). However, the pattern of AN-D inputs between GOM and CSK from Lamarque et al.,
137 (2013) shows around five times difference between the two regions, which agrees with our data.
138 Thus, in our model, we used observational data for both regions, as shown in Table 2.

139

140 *Methodology: N-mass balance model*

141 Our model consists of three sub-regions based on sampling locations during MCH cruises
142 (Figure 3), each of which contains a series of one-quarter degree square boxes, as followed by
143 Belabbassi (2006). The quarter degree boxes in this study were separated into an upper box and
144 a lower box, based on pycnocline depth, as defined by a sharp change in density and coincides
145 generally with a minimum change in oxygen concentration of 0.5 ml/L. We assume steady state
146 conditions, and estimate potential production, which we count as an estimate of potential carbon
147 flux (Figure 3a). Primary production (PP) above the pycnocline is expected to be higher than
148 below it (Anderson 1969; Sigman and Hain, 2012), which means that the two layers have
149 different biological processes. The difference in PP between upper and lower boxes also
150 depends on the freshwater discharge rate, which determines nutrient input to the upper layer,
151 seasonal variability, and transfer processes between the layers. While chlorophyll can be found
152 below the pycnocline (DiMarco and Zimmerle, 2017).

153 The N mass balance box model is modified from previous models to calculate the net
154 removal of DIN inside each box, which represents potential primary production (PPP) (De Boer
155 A.M. et al., 2010; Kim (G) et al., 2011) (Equation 1). In this model, DIN concentration
156 includes ammonium (NH₄), nitrate (NO₂), and nitrite (NO₃).

157

$$158 \quad F_{River}^{DIN} + F_{Atmo}^{DIN} + F_{Bott}^{DIN} - F_{Export}^{DIN} - F_{Deni}^{DIN} = F_{Removal}^{DIN} - \text{Eq. 1}$$

159

160 where, F_{River}^{DIN} , an input term, is DIN flux from each river discharge and calculated with C_{Box}^{DIN} ,
161 the DIN concentration in each box, A_{Bott} , the bottom area of each quarter degree box, and

162 F_{River} , river discharge rate ($C_{Box}^{DIN} \times A_{Bott} \times F_{River}$). As another input term, F_{Atmo}^{DIN} is the
163 flux from atmospheric nitrogen deposition. F_{Bott}^{DIN} , the benthic flux is additional input term in
164 the sub-pycnocline layer box. The one quarter degree blue boxes located closest to the
165 Mississippi and Atchafalaya river mouths were assumed to be the only ones affected by riverine
166 input (Figure 3b). As an output term, F_{Export}^{DIN} as an advection term was calculated from the
167 current velocity in each region from observations (Nowlin et al., 1998a, b) and from literature
168 data (Jacob et al., 2000; Lim et al., 2008) and the exchange between boxes from the residence
169 time in each box. Note that water and nutrient exchange can take place through all four sides of
170 each box, so the array is two-dimensional. F_{Export}^{DIN} for water mixing was calculated from these
171 factors; C_{EX}^{DIN} is the difference in DIN concentration between adjacent boxes, V_S is the water
172 volume of each box, and λ_{Mix} is the mixing rate of each box ($C_{EX}^{DIN} \times V_S \times \lambda_{Mix}$). We used
173 a reciprocal of the water residence time that we considered to represent horizontal mixing, i.e.
174 dispersion. Another output term is F_{Deni}^{DIN} , denitrification process from the water column, and
175 $F_{Removal}^{DIN}$ is removal by biological production. The details of the model definitions are given
176 below in Table 3 and shown in Figure 3. Each arrow indicates input (blue) and output (red)
177 terms (Figure 3). Input/output terms vary based on whether the boxes are above/below the
178 pycnocline, while there are separate inputs from the Mississippi and Atchafalaya rivers in the
179 GOM and Keum and Han rivers in the CSK, respectively.

180 In order to calculate the net removal of DIN in a box above the pycnocline layer, we used
181 our N mass balance model in Equation 2.

182

$$183 \quad F_{River}^{DIN} + F_{Atmo}^{DIN} - F_{Export}^{DIN} - F_{Sink}^{DIN} = F_{Removal}^{DIN} - \text{Eq. 2}$$

184

185 The boxes above the pycnocline layer have two input terms: 1) F_{River}^{DIN} , riverine N,
 186 which affects only a subset of boxes along the edge of each region, and 2) F_{Atmo}^{DIN} , atmospheric
 187 nitrogen deposition (AN-D), which affects every box equally. The mean value of Asian data, as
 188 shown in Table 2 (Kim (JY) et al., 2010; Luo et al., 2014; Shou et al., 2018; Zhao et al., 2015), is
 189 used for F_{Atmo}^{DIN} of the CSK region, which is initially five times higher than that of the GOM (1.4
 190 $\times 10^5$ mol day⁻¹; Wade and Sweet, 2008). We also considered vertical sinking as an input for
 191 the sub-pycnocline layer box and as an output from the upper layer. Other possible input
 192 factors might be upwelling/downwelling processes; however, these factors are neglected in the
 193 model because both regions are shallow and close inshore (Feng et al., 2014; Lim et al., 2008)
 194 and we have no observational data on upwelling/downwelling rates. The output terms are the
 195 following: 1) F_{Export}^{DIN} , the exchange rate between each box (obtained from the different N
 196 concentrations in each box and the mass transfer between them), and 2) F_{Sink}^{DIN} , removal by
 197 biological production, including sinking (assuming that any other removal factors are neglected
 198 above the pycnocline). We tested the RC02 three zone hypothesis in the upper box layer, in
 199 which we can also examine the horizontal influence (horizontal extent) of the river plume based
 200 on production rates.

201 Below the pycnocline layer we used the revised Equation 3.

202

$$203 \quad F_{Bott}^{DIN} + F_{Sink}^{DIN} - F_{Export}^{DIN} - F_{Deni}^{DIN} = F_{Removal}^{DIN} - \text{Eq. 3}$$

204

205 Equation 3 has two separate input terms; 1) The benthic flux F_{Bott}^{DIN} term contains all the
 206 potential input from the bottom sediment (defined here as net DIN release from the bottom
 207 sediment) including nutrient regeneration by bacteria, groundwater nutrient inputs, and an uptake

208 of nitrate (NO_2^-) and nitrite (NO_3^-) mainly by sedimentary denitrification (McCarthy et al., 2015;
209 Nunnally et al., 2014), and 2) F_{Sink}^{DIN} term as a vertical sinking from the box above the
210 pycnocline layer, for which we used data from Qureshi (1995). The unit of F_{Sink}^{DIN} was
211 converted to mol day^{-1} from the unit of original data ($\text{gN m}^{-2} \text{day}^{-1}$) with area of box ($0.25 \text{ m} \times$
212 0.25 m) and molar mass of N (14 g mol^{-1}).

213 In the GOM, benthic sediments provide excess ammonium to overlying water by
214 regeneration processes such as remineralization (Lehrter et al., 2012; Nunnally et al., 2014;
215 Rowe et al., 2002). Generally, there is an uptake of nitrate and nitrite mainly by sedimentary
216 denitrification (McCarthy et al., 2015) or dissimilatory nitrate reduction to ammonium (DNRA)
217 and assimilation by benthic microalgae (Christensen et al., 2000; Dalsgaard, 2003; Thornton et
218 al., 2007). Due to this, net DIN flux was used as the value of F_{Bott}^{DIN} , which shows DIN release
219 from bottom sediments to overlying water column. For example, in the GOM, the sum of
220 nitrate and nitrite fluxes to bottom sediments (e.g., May: -10.05 , July -61.9 , August: $-48.42 \mu\text{mol}$
221 $\text{N m}^{-2} \text{h}^{-1}$) were similar or smaller than the flux of ammonium from bottom sediments (e.g., May:
222 203 , July: 152 , August: $156 \mu\text{mol N m}^{-2} \text{h}^{-1}$) off Terrebonne bay (McCarthy et al., 2015). In the
223 CSK, the sum of nitrate and nitrite flux to bottom sediments and ammonium flux are $0.5 \sim 1.4$
224 $\text{mmol N m}^{-2} \text{d}^{-1}$ and $1.3 \sim 9.6 \text{ mmol N m}^{-2} \text{d}^{-1}$, respectively, which indicated that excess
225 ammonium with additional nitrate and nitrite were released from sediments in this region (Lee et
226 al., 2012). The release of nitrate and nitrite in the CSK unlike the GOM can be estimated due to
227 high inputs of nitrogen by groundwater in the CSK (Kim (G) et al., 2011) even though there is
228 minor uptake of nitrate and nitrite. Diffusion from groundwater can probably be ignored in the
229 GOM as Rabalais et al. (2002) reported that the groundwater discharge is very low in coastal
230 Louisiana, but is likely important elsewhere and is known to be important in the CSK. Based

231 on this, we averaged and sum the fluxes data of nitrate, nitrite, and ammonium from McCarthy et
232 al., 2015 for the GOM and Lee et al., 2012 for the CSK, respectively, and then applied
233 F_{Bott}^{DIN} value as $1.2 \text{ mmol N m}^{-2} \text{ day}^{-1}$ in the GOM and $6.2 \text{ mmol N m}^{-2} \text{ day}^{-1}$ in the CSK. Thus,
234 in equation 3, the benthic flux term is calculated from existing literature results after considering
235 all DIN fluxes as above (Lee et al., 2012; McCarthy et al., 2015), and then multiplied by the area
236 of each box.

237 The output terms are; 1) F_{Export}^{DIN} , the exchange rate between each box in the lower layer,
238 and 2) F_{Deni}^{DIN} , the denitrification rate from the water column. Due to high stratification at the
239 pycnocline, upward transfer of dissolved material from the lower layer to the upper layer is
240 assumed not to occur in our model. Also, denitrification from the water column below the
241 pycnocline is a significant N removal process, which removes up to a maximum 68% of total N
242 input from the Mississippi River in the GOM (McCarthy et al., 2015). As the value of F_{Deni}^{DIN}
243 in the GOM, we used a direct measurement of denitrification rates from the McCarthy et al.,
244 (2015) in the water column ($88 \mu\text{mol m}^{-2} \text{ h}^{-1}$, which converted to $2.1 \text{ mmol N m}^{-2} \text{ day}^{-1}$) where
245 the stations were exactly same as our sub-region A, B, and C. We assumed this applied only
246 below the pycnocline where oxygen concentrations decrease. However, in the CSK, there is no
247 water column denitrification data because the dissolved oxygen concentration has never been
248 down below about 4 mg L^{-1} during our data periods. Based on this, we estimated that there is a
249 very little water column denitrification in the CSK, so we did not count this term in the CSK.
250 Thus, we only considered the sedimentary denitrification term for the CSK region.

251 Water transport in the region is generally from the east, i.e., from near the Mississippi
252 River in Sub-region A to the west, near the Atchafalaya River in Sub-region C during non-
253 summer periods. During summer, the winds change direction from easterly to westerly,

254 blocking the water flow to the west (Cho et al., 1998). We calculated advection from current
255 meter data collected during the LATEX program (Nowlin et al., 1998a, b) from April 1992 to
256 December 1994, from which we determined U (west to east flow) and V (south to north flow)
257 components (cm s^{-1}). Figure 4 shows the mean values of coastal ocean current velocities. The
258 annual range of the currents is 0 to 30 cm s^{-1} for the longshore component, with standard
259 deviation of about 8 cm s^{-1} , and 0 to 7 cm s^{-1} for the cross-shelf component, with a similar
260 standard deviation, but these current velocities are not constant and change depending on time
261 and day. The annual current velocities in the CSK are more affected by tidal exchange and the
262 presence of the Yellow Sea Current, but velocities are similar to those in the GOM (Jacob et al.,
263 2000; Lim et al., 2008). The annual range of the currents is around 0 to 28 cm s^{-1} and 0 to 7 cm
264 s^{-1} for the cross-shelf component. Thus, we used the mean value of the current velocity for the
265 time of year during each cruise in both the GOM and the CSK for calculating the advective flow
266 in both alongshore and onshore/offshore directions.

267 To run the box model, we assumed three factors: 1) the study area is in a steady state
268 condition, with equal input sources and outputs, 2) AN-D is evenly distributed across each area,
269 and 3) DIN is fully utilized by phytoplankton growth in the layer above the pycnocline, so we
270 can neglect other removal factors. However, in the layer below the pycnocline, as we
271 mentioned above, denitrification, which leads to a main loss of DIN as nitrogen gas, is
272 considered as another output term in Equation 3. Because we assumed that all DIN removed is
273 fully consumed by primary production above the pycnocline, we can calculate potential carbon
274 fluxes and oxygen consumption using the Redfield ratio (C: N: O: P = 106: 16: 138: 1). The
275 PPP can be compared with ^{14}C measurement data (Lohrenz et al., 1998, 1999; Redalje et al.,
276 1994; Quigg et al., 2011) and dissolved oxygen data from MCH mooring C at 29° N, 92° W

277 (4/3/2005 ~ 7/10/2005) (Bianchi et al., 2010).

278

279 **Results**

280 *An N-mass balance model for the Texas-Louisiana Shelf*

281 The existence of the three zones suggested by RC02 has been verified from winter data
282 using nutrient/salinity relationships (Kim 2018). Figure 5 shows the contour graph based on the
283 mean concentration of DIN at each station during the MCH M4 (March 2005) cruise. For
284 operational and modeling purposes, stations were grouped into three sub-regions – near the
285 Mississippi (A), near the Atchafalaya (C) and an intermediate region (B) between ~90°-91°W.
286 During summer, it is hard to use nutrient/salinity relationships directly because riverine nutrient
287 inputs are lower and phytoplankton growth causes rapid nutrient consumption over the shelf,
288 leading to low overall nutrient surface concentrations. We calculated the mean [DIN] in each
289 box, and then used the relationship between DIN and salinity to define the edges of the three
290 zones. Near the coast salinity was consistently low, with high turbidity from the river water
291 discharge. This was labelled the brown (river) zone.

292 A range of N input values from various sources were used in the N mass balance model
293 to estimate PPP and carbon fluxes in the coastal GOM. The PPP rates were highest near the
294 river mouth and we set the boundaries of production for each zone based on our N mass balance
295 model results and mean [DIN] data. We defined the PPP rate of the brown zone as being over 2
296 $\text{gC m}^{-2} \text{ day}^{-1}$ because of the high input of N from the river, AN-D, and benthic fluxes, and the
297 rate in the blue zone is less than $0.1 \text{ gC m}^{-2} \text{ day}^{-1}$. The PPP rate in the green zone is then
298 between 0.1 and $2 \text{ gC m}^{-2} \text{ day}^{-1}$. Basically, these PPP ranges were set based on synthesized
299 measured ranges of coastal GOM primary production, as defined for near, mid, and far fields of

300 the coastal GOM (Dagg and Breed 2003; Lohrenz et al., 1999). Note that our model results of
301 the PPP might overestimate the actual production because of light limitation, following RC02.

302 The edges of the three zones above and below the pycnocline layer, based on our N mass
303 balance model results, are shown in Figures 6a and b. The patterns of the boundaries above and
304 below the pycnocline differ from the edges of the zones. The brown zone was found above the
305 pycnocline on all cruises close to the Mississippi River mouth because of the high nutrient
306 concentrations, but only appeared off the Atchafalaya River in March 2005 (MCH M4).
307 However, below the pycnocline it was found only in April 2004 (MCH M1) in sub-region A.
308 This suggests that vertical transport across the pycnocline rapidly removes the high levels of
309 suspended material that cause light limitation above the pycnocline. In the green zones, the
310 nutrient source is mostly supported directly by the river, with minor additional sources of N from
311 vertical sinking, AN-D, and benthic fluxes. We utilized the vertical sinking flux from the
312 sediment trap data from Qureshi (1995) below the pycnocline layer to estimate PPP. This
313 varied between 0.1-1.0 gN m⁻² day⁻¹ (Table 3). Typically, in the blue zone where biological
314 production is low, vertical sinking followed by local decomposition is assumed to be the major
315 factor that changes the nutrient concentration in the lower layer. The blue zone is always more
316 extensive below the pycnocline than above it, which suggests there is little or no sub-pycnocline
317 production except close to the coast and/or the river mouths, and reinforces the assumption that
318 any chlorophyll below the pycnocline is inactive (Figure 6b). Thus, we can identify the
319 horizontal influence of the river plume in the layer below the pycnocline and the variation in the
320 boundaries of the three zones, based on the observed nutrient data from a bottom layer and our N
321 mass balance model. The model suggests that regions of moderate potential productivity
322 extend offshore at least as far as 28° 30'N in sub-region B, both above and below the pycnocline.

323

324 *An N mass balance model calibration*

325 The model calibration was done with historic literature data. Literature data suggest that
326 observed PP rates in the green and brown zones of the coastal GOM vary between 0.4 gC m⁻²
327 day⁻¹ (winter) and ~ 8 gC m⁻² day⁻¹ (summer) (Dagg et al., 2007; Lohrenz et al., 1998, 1999;
328 Redalje et al., 1994). Recently, Quigg et al. (2011) measured the integrated PP rates with ¹⁴C
329 measurements during 2004 in the coastal GOM. The highest integrated PP rates were found
330 near the Mississippi River at 3.5 gC m⁻² day⁻¹ (in July), and near the Atchafalaya River at 2.7 ~
331 5.9 gC m⁻² day⁻¹ (in May to July) (in the brown and green zones). However, lowest integrated
332 PP rates were on the outer part of the LATEX shelf (the blue zone) at 0.07 gC m⁻² day⁻¹ (in
333 March), 0.04 ~ 0.15 gC m⁻² day⁻¹ (in May), and 0.33 ~ 0.91 gC m⁻² day⁻¹ (in July). Additionally,
334 Quigg et al., (2011) pointed out that these higher PP values were affected by high riverine
335 nutrients input from the MR that flows westward during that time period.

336 The actual PP ranges were similar with our model-based PPP (Figure 6). However, this
337 was different from RC02's brown zone. This might be due to the differences between methods
338 such as ¹⁴C, our N-mass balance model, and RC02's theoretical model. Typically, RC02
339 assumed that the brown zone is light limited due to high sediment turbidity, but our model does
340 not account for this and only considered DIN concentrations. Except for this, our PPP results
341 are similar to direct productivity measurements from the ¹⁴C incubations (Quigg et al., 2011).
342 Our model result (PPP) showed the same range of values as ¹⁴C incubations (e.g., Dagg et al.,
343 2007; Lohrenz et al., 1998, 1999; Quigg et al., 2011; Redalje et al., 1994) in the three sub-
344 regions.

345 Note that our model assumed all the biological uptake could be converted directly to

346 production rates, which we considered as PPP. The PPP from cruises MCH M1 ~ M8 for
347 samples from above the pycnocline calculated using our model is reasonable based on
348 comparison with previous PP values (Figure 6a). The PPP ranges (0.01 ~ 5.05 gC m⁻² day⁻¹)
349 were similar to previous ¹⁴C measurement PP values of between 0.04 ~ 5.9 gC m⁻² day⁻¹.

350 Based on our model calculation, which assumes all the nutrients are available for
351 production, the PPP showed maxima at all times in sub-region A (near the Mississippi river) and
352 minima in sub-region B (between the Mississippi and Atchafalaya River), except for MCH M2 in
353 June 2004, when sub-region C had the lowest PPP (Figure 6a). The high values in sub-region A
354 are due largely to underutilization of nutrients in regions of high turbidity. As the water flows
355 west under the influence of the Coriolis effect, PPP is expected to decrease as a result of
356 declining nutrient concentrations because of dilution and nutrient uptake during biological
357 production while the water flows to sub-region B. In sub-region C, MCH M4 (March 2005)
358 had the highest PPP among the all MCH cruises. This probably depended on high nutrient
359 concentrations being present during the winter period, when the region was affected by
360 Atchafalaya River nutrient input.

361

362 *Model scenarios in the Gulf of Mexico (GOM)*

363 We tested the sensitivity of the model to changes in input/output parameters such as
364 increasing AN-D and decreasing riverine N input. Assuming the model is robust, we
365 investigated three model scenarios based on the nutrient distributions seen during the MCH1
366 cruise (note that using data from other cruises gives very similar results). In the first scenario,
367 we cut riverine N input 60% and increased the AN-D input by a factor of two based on
368 increasing N emission predictions (Duce et al., 2008; He et al., 2010; Kanakidou et al., 2016;

369 Kim (T) et al., 2011; Lawrence et al., 2000; Paerl et al., 2002). In the second scenario, we
370 doubled the amount of AN-D as in scenario 1 and decreased riverine N input by 30% based on
371 the hypoxia management plan goal (Gulf Hypoxia Action Plan Report, 2005, 2008; Rabalais et al.
372 2009). In the third scenario, we increased riverine N input by 20%, assuming the failure of the
373 hypoxia management plan, while we set the AN-D amount equal with the first and second
374 scenarios. Based on our N-mass balance model calculation and model scenarios, we can
375 initially estimate carbon fluxes from our PPP rate, and, using the Redfield carbon to oxygen
376 stoichiometry ratio (106:138), the overall oxygen balance within the coastal GOM (Table 4).

377 As can be seen in the scenario results for MCH M1 data (Table 4), the riverine N input
378 source is still the major controlling factor in the coastal GOM region even when its contribution
379 is greatly reduced and the AN-D source is doubled. For instance, if we fail to reduce riverine N
380 input in the future (scenario 3), the potential carbon fluxes will increase by 17% relative to
381 current conditions. In contrast, the AN-D input source only increased to a maximum of 5% of
382 the total input term and this indicates that AN-D input is still a minor factor in the GOM. If the
383 production is increased, overall oxygen demand will also be increased. The MCH M1 scenario
384 result indicated that the overall oxygen demand would increase approximately 21% if we fail to
385 reduce riverine N input, likely increasing considerably the area of the hypoxia.

386

387 *An N mass balance model in the Coastal Sea off Korea (CSK)*

388 As we have done in the GOM, we used our N mass balance model to estimate the PPP in
389 the CSK and define the three different zones (Figure 7). Similar to the GOM region, the PPP
390 rates were highest near the river mouth, and we set the boundaries of each zone based on our N-
391 mass balance model results. Based on nutrient data, as was done for the GOM, we defined the

392 brown zone as having a PPP rate above $1.5 \text{ gC m}^{-2} \text{ day}^{-1}$ because of the increased N sources from
393 the river, AN-D, and the sediment flux. We defined the green zone as having PPP rates between
394 0.3 to $1.5 \text{ gC m}^{-2} \text{ day}^{-1}$ and the blue zone as having rates of less than $0.3 \text{ gC m}^{-2} \text{ day}^{-1}$.

395 The seasonal results shown in Figures 7a and b show that the boundaries of the three
396 zones above and below the pycnocline layer were roughly consistent with the main change
397 coming in summer (August), which is the wet season and sees the highest river discharge. The
398 large size of the green zone in all seasons suggests that AN-D is consistently adding extra
399 nitrogen to the surface ocean along with the riverine N input. This is supported by the fact that
400 the PPP in the blue zone is an order of magnitude higher than for the GOM. Around 90% of the
401 grid cells in the CSK are in the same zones above and below the pycnocline (Figure 7 a and b)
402 during all four cruises; however, in the GOM (Figure 6 a and b) this was found for fewer than
403 half of the grid cells. This is probably due to the difference in freshwater discharge rate in the
404 two regions, which leads to a much larger stratified area in the GOM than in the CSK.

405 One question that has not been investigated is the temperature dependence of primary
406 productivity in the two areas. While the GOM is temperate throughout the year, winter
407 temperatures in the CSK fall to $\sim 5^\circ\text{C}$. However, according to the ocean color remote sensing
408 images from near the CSK river mouth reported by Son et al., (2005), primary production in the
409 CSK does not appear to be strongly affected by temperature. The PPP results of our model (0.2
410 to $2.2 \text{ gC m}^{-2} \text{ day}^{-1}$) agreed with their ocean color remote sensing results (0.4 to $1.6 \text{ gC m}^{-2} \text{ day}^{-1}$)
411 in the CSK. Also, during all seasons, the Keum River consistently supplies high amounts of
412 DIN (average: $< 60 \mu\text{M}$) (Lim et al., 2008) to the coastal zone (especially close to the Keum
413 mouth). We believe, therefore, that the higher value of PPP in winter near the Keum mouth
414 (brown zone in figure 7a), is reasonable.

415 The AN-D input source comes mainly from the Chinese side of the East China Sea (ECS)
416 and this affects the boundaries of the green and blue zones above the pycnocline as it is deposited
417 uniformly across the region. There is also nutrient input from offshore, as the Yellow Sea
418 Bottom Cold Water Mass can up-well during the mixing process and is assumed to supply
419 additional nutrients to the outer shelf (Lim et al., 2008).

420

421 *Model scenarios in Mid-Western Coastal Sea off Korea (CSK)*

422 AN-D is currently considerably more important (by approximately an order of magnitude)
423 in the CSK than in the GOM), and it is anticipated that AN-D will likely be a major controlling
424 factor here in the future (Duce et al., 2008; He et al., 2010; Kim (T) et al., 2011; Lawrence et al.,
425 2000; Paerl et al., 2002). Because of the lack of research on potential hypoxia scenarios in
426 Korea, we used the same three scenarios in the CSK as were used for the GOM. Similar to
427 GOM results, riverine N input remains the major controlling factor; however, in this area, the
428 AN-D source is more critical than in the GOM region (Table 5). The AN-D input source
429 increased from 20% to 47% of the total input under scenario 1, while based on our scenario 3
430 results, increases in the AN-D input source and riverine N input together will affect biological
431 production by increasing carbon fluxes up to 25% and oxygen demand up to 32% if we fail to
432 reduce N input in future (Table 5).

433

434 **Discussion**

435 Most previous model studies in the GOM were focused on predicting the hypoxia area
436 (Bierman et al., 1994; Fennel et al., 2011, 2013; Justic et al., 1996, 2002, 2003; Scavia et al.,
437 2004). For example, Justic et al., (1996; 2003) used a two-layer model incorporating vertical

438 oxygen data, from one station (LUMCON station C6; 28.867°N, 90.483°W), to predict the size
439 of the hypoxia area. Similarly, Fennel et al. (2011; 2013) used her more complex simulation
440 model, which included oxygen concentration as well as a plankton model from Fasham et al.
441 (1990), to predict the size of the hypoxia region in the GOM. Our N mass balance model, in
442 contrast, uses historical data from the LATEX shelf to estimate potential carbon fluxes in the
443 GOM, and calculate the overall oxygen demand from those carbon fluxes. While this affects
444 the total area subject to hypoxia it does not estimate the size of the hypoxic zone.

445 In contrast to our model, traditional predictive models have also ignored different
446 nitrogen input sources such as AN-D and SGD. While this is probably reasonable on the Texas-
447 Louisiana shelf, where riverine inputs dominate, it may not apply in other coastal regions. As a
448 result, model studies in this region have concluded that reducing riverine N input is the only
449 solution to decrease the size of the hypoxia area in the GOM (Gulf Hypoxia Action Plan Report,
450 2005, 2008; Rabalais et al. 2009; Scavia et al., 2013). According to our model results, AN-D is
451 still a minor controlling factor in the GOM; however, in the CSK, the AN-D contributed more to
452 the total nitrogen budget and may be a major controlling factor in the future. This indicates that
453 AN-D should be considered as another input term for nutrient managements, especially in Asia
454 or in other regions where high concentrations are expected. Similarly, nitrogen input from
455 either sediment fluxes or groundwater also need to be considered.

456 Our zonal boundaries can be compared with the results of Lahiry (2007), who used
457 salinity to define the edges of each zone for the three cruises MCH M1, M2, and M3 (Figure 8)
458 and defined the edges of the RC02 zones in the coastal GOM based solely on salinity. Her
459 limited simulation results indicated similar patterns to our model based on DIN concentration
460 near the Mississippi River mouth (e.g., during MCH M1, M2, and M3). Mixing was more

461 conservative in this region than further west because the low salinity water with high nutrients
462 was less diluted with offshore water.

463 Away from the MR in sub-regions B and C, however, her results gave very different
464 boundaries for the three zones compared with our results (Figure 8). In particular, the results
465 near the Atchafalaya River were very different (compare Figures 6 and 8). For example, our
466 data showed only green and blue zones off Atchafalaya Bay during MCH M1, with no brown
467 zone. Similarly, the extent of the blue zones in sub-region C during MCH M2 and M3 is also
468 very different. We believe that our DIN-model based classification can cover more complex
469 biological processes than the Lahiry (2007) method, which considers only advection and mixing
470 and the DIN-model is a more sensible way to look at biological processes in the GOM.

471 Our results also agree with previous studies that demonstrated that both the GOM and
472 CSK regions are N-limited for most of the year (Kim (G) et al., 2011; Turner and Rabalais, 2013).
473 This compares with the results of Sylvan et al., (2007), who reported that the coastal GOM could
474 be P-limited in the MR delta mouth area where our brown zone is located, while RC02 suggested
475 light-limitation rather than N- or P-limitation. However, this P-limited condition appears to
476 occur when N concentrations are very high. In particular, the N/P ratios in the both the GOM
477 and CSK during our sampling were less than 16, indicating that both regions were N-limited,
478 although a few stations in the brown zone near the MR river area had ratios of between 16 and
479 18 (Figure 9). These higher N/P ratios may result from the high sediment turbidity causing
480 light-limited conditions in this zone near the river mouth (Rowe and Chapman, 2002).

481 It should be remembered, however, that the arithmetic N:P value per se is unimportant in
482 determining nutrient limitation. As long as both nutrients can be measured, it is theoretically
483 possible for phytoplankton to continue to grow. The MARS has generally such an excess of N

484 relative to P that N:P ratios $\gg 16$ can be expected as P concentrations fall, but this does not
485 necessarily mean that productivity is limited, and we never found P concentrations of zero in any
486 of our sub-regions; the lowest P concentration measured during all cruises in the GOM and CSK
487 was 0.2 μM .

488 Both the GOM and CSK regions receive nitrogen inputs from AN-D, rivers, and benthic
489 fluxes. These different nitrogen input sources control coastal productivity, and this may reflect
490 the different nitrogen cycling in the two regions. In the GOM, the riverine N input source
491 consistently dominates coastal productivity and eutrophication, while, in the CSK, AN-D is also
492 becoming a critical controlling factor. In the CSK, however, there is strong tidal mixing of
493 freshwater from the Keum River and/or Gyunggi Bay with nearby coastal water, which results in
494 a tidal front along the offshore region and off the Taean Peninsula during spring and summer. It
495 is this physical mixing that mostly controls the spatial distribution patterns of nutrients and
496 salinity here, particularly below the pycnocline (Lim et al., 2008). The brown zone in the upper
497 layer in the CSK (August 2008) changed to a green zone region below the pycnocline layer as a
498 result of the strong coastal tidal mixing.

499 RC02 considered their model to be theoretical. In the brown zone, close to the river
500 mouth, they assumed turbidity leads to light-limited conditions. Their results agree well with
501 measured ^{14}C PP numbers from Quigg et al. (2011) who found the lowest integrated PP is near
502 the MR delta mouth. However, our N mass balance model did not consider light limitation and
503 therefore PPP in the brown zone is high. Such good agreement suggests that our model can be
504 applied to a wide region, while ^{14}C measurements are typically conducted at a few specific points,
505 as long as such limitations are taken into account.

506 In the CSK, most previous production studies focused on inshore areas such as estuaries

507 or rivers. Our research focused for the first time on the coastal ocean off Korea. Our results
508 explained that diverse nitrogen sources need to be recognized as potential issues for future
509 nutrient management concerned with hypoxia, eutrophication, or other environmental
510 issues. The agreement between our results and the pattern of production based on satellite-
511 sensing in the CSK (Son et al., 2005), suggests that our model is reasonable.

512 The results of our changing scenarios represent how the biological processes in these
513 coastal regions may vary as individual nutrient sources change; in the near future both AN-D
514 flux and riverine N flux need to be considered for managing nitrogen in coastal waters. While
515 our model cannot predict the area of the hypoxic zone, we can investigate the effects of potential
516 flux changes of each factor, such as AN-D, riverine input, or benthic fluxes, and calculate the
517 effects of changes in each on PPP and on the overall oxygen balance for the region. We have
518 only considered different input terms of our N mass balance model; output terms such as water
519 mixing rates and the residence time for each box need more detailed study in future work to
520 calculate more realistic production changes in each box.

521

522 **Conclusion**

523 The model suggests that the three zone theory of RC02 can be applied not only in the
524 northern GOM but also in the CSK region and that three zones can be distinguished based on
525 their nutrient concentration. As a result, we believe that using our N mass balance model to
526 separate different zones based on RC02 may be appropriate not only for large-scale regions like
527 the GOM and CSK but also at small scales such as river or estuary systems. The model also
528 estimates potential primary production and carbon flux based on the inclusion of AN-D data that
529 have not been considered previously (e.g. Bierman et al., 1994; Kim (T) et al., 2011). Our

530 results agree well with previous ^{14}C measurements in the GOM (Quigg et al., 2011) and ocean
531 color remote sensing in the CSK (Son et al., 2005).

532 Based on CSK cruise data results, we can initially determine where the three different
533 zones are in the CSK. We identified the brown zone close to the Keum River mouth and the
534 green and blue zones further away from the coast of Korea.

535 We evaluated our model and tested its sensitivity based on three different scenarios.
536 Through our scenario results, we assume that the AN-D is a considerable factor in the CSK as
537 well as the riverine N input from the Keum river. Reducing nutrient input from the river is
538 critical for hypoxia management policy (Gulf Hypoxia Action Plan Report, 2005, 2008; Rabalais
539 et al. 2009). In addition, these model scenarios will be helpful in future coastal nutrient
540 management or hypoxia management studies in the CSK, especially as AN-D sources become
541 more important.

542

543 **Acknowledgements**

544 The authors would like to thank to the captain and crew of the R/V Gyre along with the
545 marine technicians and students who participated in the cruises. This project was funded by
546 NOAA Center for Sponsored Coastal Ocean Research, Grant Numbers: NA03NOS4780039,
547 NA06NOS4780198, and NA09NOS4780208.

548

549 **References**

- 550 Anderson, G. C.: Subsurface chlorophyll maximum in the northeast Pacific Ocean. *Limnology*
551 *and Oceanography.*, 14(3), 386-391, 1969.
- 552
- 553 Alexander, R. B., Smith, R. A., Schwartz, G. E., Preston, S. D., Brakebill, J. W., Srinivasan, R.,
554 and Pacheco, A. P.: Atmospheric nitrogen flux from the watersheds of major estuaries of
555 the United States: An application of the SPARROW watershed model., 119-170, 2000.
- 556
- 557 Alexander, R. B., Smith, R. A., Schwarz, G. E., Boyer, E. W., Nolan, J. V., and Brakebill, J. W.:
558 Differences in phosphorus and nitrogen delivery to the Gulf of Mexico from the
559 Mississippi river basin. *Environmental Science and Technology.*, 42, 822-830, 2008.
- 560
- 561 Belabbassi, L.: Examination of the relationship of river water to occurrences of bottom water
562 with reduced oxygen concentrations in the northern Gulf of Mexico. Texas A & M
563 University. Ph.D. Dissertation., 2006.
- 564
- 565 Bianchi, T. S., DiMarco, S. F., Cowan, Jr. JH., Hetland, R. D., Chapman, P., Day, J. W., and
566 Allison, M. A.: The Science of hypoxia in the Northern Gulf of Mexico: A review.
567 *Science of the total Environment.*, 408(7), 1471-1484, 2010.
- 568
- 569 Bierman, V. J., Hinz, S. C., Wiseman, Jr. W. J., Rabalais, N. N., and Turner, R. E.: A
570 Preliminary Mass Balance Model of Primary Productivity and Dissolved Oxygen in the
571 Mississippi River Plume/Inner Gulf Shelf Region. *Estuaries.*, 17(4), 886-899, 1994.
- 572
- 573 Bode, A., and Dortch, Q.: Uptake and regeneration of inorganic nitrogen in coastal waters
574 influenced by the Mississippi River: spatial and seasonal variations. *Journal of Plankton*
575 *Resources.*, 18, 2251-2268, 1996.
- 576
- 577 Castro, M. S., Driscoll, C. T., Jordan, T. W., Reay, W. G., Boynton, W. R., Seitzinger, S. P.,
578 Styles, R. V., and Cable, J. E.: Contribution of atmospheric deposition to the total
579 nitrogen loads to thirty-four estuaries on the Atlantic and Gulf coasts of the United States,
580 77-106, 2000.
- 581
- 582 Castro, M. S., and Driscoll, C. T.: Atmospheric nitrogen deposition to estuaries in the mid-
583 Atlantic and northeastern United States. *Environmental science & technology.*, 36(15),
584 3242-9, 2002.
- 585
- 586 Cho, K. R., Reid, O., and Nowlin, Jr W. D.: Objectively mapped stream function fields on the
587 Texas-Louisiana shelf based on 32 months of moored current meter data. *Journal of*
588 *Geophysics Research.*, 103(C5), 10377-10390, 1998.
- 589
- 590 Choi, H. Y., Lee, S. H., and Oh, I. S.: Quantitative Analysis of the Thermal Front in the Mid-
591 Eastern Coastal Area of the Yellow Sea. *Journal of the Korean Society of Oceanography*
592 *[The Sea].*, 3, 1-8, 1998.
- 593

- 594 Choi, H. Y., Lee, S. H., and Yoo, K. Y.: Salinity Distribution in the Mid-eastern Yellow Sea
595 during the High Discharge from the Keum River Weir. *Journal of the Korean Society of*
596 *Oceanography [The Sea]*, 4, 1-9, 1999.
597
- 598 Christensen, P. B., Rysgaard, S., Sloth, N. P., Dalsgaard, T., and Schwaerter, S.: Sediment
599 mineralization, nutrient fluxes, denitrification and dissimilatory nitrate reduction to
600 ammonium in an estuarine fjord with sea cage trout farms. *Aquatic Microbial Ecology*,
601 21, 73-84, 2000.
602
- 603 Cornell, S., Rendell, A., and Jickells, T.: Atmospheric inputs of dissolved organic nitrogen to the
604 oceans. *Nature*, 376, 243-246, 1995.
605
- 606 Dagg, M. J., and Breed, G. A.: Biological effects of Mississippi River nitrogen on the northern
607 Gulf of Mexico-a review and synthesis. *Journal of Marine Systems*, 43, 133-152, 2003.
608
- 609 Dagg, M. J., Ammerman, J. W., AMON, R. M. W., Gardner, W. S., Green, R. E., Lohrenz, S. E.:
610 A review of water column processes influencing hypoxia in the northern Gulf of Mexico.
611 *Estuaries Coasts*, 30, 735-752, 2007.
612
- 613 Dalsgaard, T.: Benthic primary production and nutrient cycling in sediments with benthic
614 microalgae and transient accumulation of macroalgae. *Limnology and Oceanography*,
615 48(6), 2138-2150, 2003.
616
- 617 De Boer, A. M., Watson, A. J., Edwards, N. R., and Oliver, K. I. C.: A multi-variable box model
618 approach to the soft tissue carbon pump. *Climate of the past*, 6, 827-841, 2010.
619
- 620 Diaz, R. J., and Rosenberg, R.: Marine benthic hypoxia: A review of its ecological effects and
621 the behavioural responses of benthic macrofauna. *Oceanography Marine Biology. Ann.*
622 *Rev.*, 33, 245-303, 1995.
623
- 624 Diaz, R. J., and Rosenberg, R.: Spreading dead zones and consequences for marine ecosystems.
625 *Science*, 321(5891), 926-9, 2008.
626
- 627 DiMarco, S. F., and Zimmerle, H. M.: MCH Atlas: Oceanographic Observations of the
628 Mechanisms Controlling Hypoxia Project. Texas A&M University, Texas Sea Grant,
629 College Station, TX. Publication TAMU-SG- 17-601,350. ISBN 978-0-692-87961-0,
630 2017.
631
- 632 Dodds, W. K., and Smith, V. H.: Nitrogen, phosphorus, and eutrophication in streams. *Inland*
633 *Waters*, 6, 155-164, 2016.
634
- 635 Doney, S. C., Mahowald, N., Lima, L., Feely, R. A., Mackenzie, F. T., Lamarque, J. F., and
636 Rasch, P. J.: Impact of anthropogenic atmospheric nitrogen and sulfur deposition on
637 ocean acidification and the inorganic carbon system. *Proceedings of the National*
638 *Academy of Science*, 104, 14580-14585, 2007.
639

640 Dortch, Q., and Whittedge, T. E.: Does nitrogen or silicon limit phytoplankton in the Mississippi
641 River plume and nearby regions? *Continental Shelf Research.*, 12, 1293-1309, 1992.
642

643 Duce, R. A., LaRoche, J., Altierl, K., Arrigo, K. R., Baker, A. R., Capone, D. G., Cornell, S.,
644 Dentener, F., Galloway, J., Ganeshram, R. S., Geider, R. J., Jickells, T., Kuypers, M. M.,
645 Langlois, R., Liss, P. S., Liu, S. M., Middelburg, J. J., Moore, C. M., Nickovic, S.,
646 Oschlies, A., Pedersen, T., Prospero, J., Schlitzer, R., Seitzinger, S., Sorensen, L. L.,
647 Uematsu, M., Ulloa, O., Voss, M., Ward, B., and Zamora, L.: Impacts of Atmospheric
648 Anthropogenic Nitrogen on the Open Ocean. *Science.*, 320, 893-897, 2008.
649

650 Fasham, M. J. R., Ducklow, H. W., and Mckelvie, S. M.: A nitrogen-based model of plankton
651 dynamics in the oceanic mixed layer. *Journal of Marine research.*, 48 ,591-639, 1990.
652

653 Feng, Y., DiMarco, S. F., and Jackson, G. A.: Relative role of wind forcing and riverine nutrient
654 input on the extent of hypoxia in the northern Gulf of Mexico. *Geophysical Research*
655 *Letters.*, 39, L09601, 2012.
656

657 Feng, Y., Fennel, K., Jackson, G. A., DiMarco, S. F., and Hetland, R. D.: A model study of the
658 response of hypoxia to upwelling-favorable wind on the northern Gulf of Mexico shelf.
659 *Journal of Marine Systems.*, 131, 63-73, 2014.
660

661 Fennel, K., Wilkin, J., Levin, J., Moisan, J., O'Reilly, J., and Haidvogel, D.: Nitrogen cycling in
662 the Middle Atlantic Bight: Results from a three-dimensional model and implications for
663 the North Atlantic nitrogen budget. *Global Biogeochemical cycles.*, 20, GB3007,
664 doi:10.1029/2005G, 2006.
665

666 Fennel, K., Hetland, R. D., Feng, Y., and DiMarco, S. F.: A coupled physical-biological model
667 of the Northern Gulf of Mexico shelf: model description, validation and analysis of
668 phytoplankton variability. *Biogeosciences.*, 8, 1881-1899, 2011.
669

670 Fennel, K., Hu, J., Laurent, A., Marta-Almeida, M., and Hetland, D. R.: Sensitivity of hypoxia
671 predictions for the northern Gulf of Mexico to sediment oxygen consumption and model
672 nesting. *Journal of Geophysical Research: Oceans.*, 118, 990-1002, 2013.
673

674 Forrest, D. R., Hetlandl R. D., and DiMarco, S. F.: Multivariable statistical regression models of
675 the areal extent of hypoxia over the Texas–Louisiana continental shelf. *Environmental*
676 *Research Letters.*, 6, 045002, 2011.
677

678 Goolsby, D. A. Mississippi basin nitrogen flux believed to cause Gulf hypoxia., *EOS*
679 *Transactions* 2000:29–321, 2000.
680

681 Green, R. E., Gould, Jr. R. W., and Ko, D. S.: Statistical models for sediment/detritus and
682 dissolved absorption coefficients in coastal waters of the northern Gulf of Mexico.
683 *Continental Shelf Research.*, 28(10), 1273-1285, 2008.
684

685 Gulf Hypoxia Action Plan Report. Mississippi River Gulf of Mexico Watershed Nutrient Task
686 Force., 2005.

687

688 Gulf Hypoxia Action Plan Report. Mississippi River Gulf of Mexico Watershed Nutrient Task
689 Force., 2008.

690

691 Hagy, J. D., Sanford, L. P., and Boynton, W. R.: Estimation of net physical transport and
692 hydraulic residence times for a coastal plain estuary using box models., *Estuaries*
693 23:328–340. doi:10.2307/1353325, 2000.

694

695 He, C. H., Wang, X., Liu, X., Fangmeyer, A., Christie, P., and Zhang, F.: Nitrogen deposition and
696 its contribution to nutrient inputs to intensively managed agricultural ecosystems.
697 *Ecological Application.*, 20(1), 80-90, 2010.

698

699 Hetland, R. D., and DiMarco, S. F.: How does the character of oxygen demand control the
700 structure of hypoxia on the Texas-Louisiana continental shelf? *Journal of Marine*
701 *Systems.*, 70, 49-62, 2008.

702

703 Howarth, R. W., and Marino, R.: Nitrogen as the limiting nutrient for eutrophication in coastal
704 marine ecosystems: Evolving views over three decades. *Limnology and Oceanography.*,
705 51(1), 364-376, 2006.

706

707 Jacob, G. A., Hur, H. B., and Riedlinger, S. K.: Yellow and East China Seas response to winds
708 and currents. *Journals of Geophysical Research.*, 105 (21), 947-968, 2000.

709

710 Justic, D., Rabalais, N. N., and Turner, R. E.: Effects of climate change on hypoxia in coastal
711 waters; A doubled CO2 scenario for the northern Gulf of Mexico. *Limnology and*
712 *Oceanography.*, 41(5), 992-1003, 1996.

713

714 Justic, D., Rabalais, N. N., and Turner, R. E.: Modeling the impacts of decadal changes in
715 riverine nutrient fluxes on coastal eutrophication near the Mississippi River Delta.
716 *Ecological Modelling.*, 152, 33-46, 2002.

717

718 Justic, D., Rabalais, N. N., and Turner, R. E.: Simulated responses of the Gulf of Mexico
719 hypoxia to variations in climate and anthropogenic nutrient loading. *Journal of Marine*
720 *Systems.*, 42, 115-126, 2003.

721

722 Kanakidou, M., Myriokefalitakis, S., Daskalakis, N., and Fanourgakis, G.: Past, Present, and
723 Future Atmospheric Nitrogen Deposition. *American Meteorological Society.*, 73(5),
724 2039-2047, 2016.

725

726 Kim, G., Kim, J. S., and Hwang, D. W.: Submarine groundwater discharge from oceanic islands
727 standing in oligotrophic oceans: Implications for global production and organic carbon
728 fluxes. *Limnology and Oceanography.*, 56(2), 673-682, 2011.

729

730 Kim, J. S., Lee, M. J., Kim, J., and Kim, G.: Measurement of Temporal and Horizontal
731 Variations in ²²²Rn Activity in Estuarine Waters for Tracing Groundwater Inputs.
732 Ocean Science Journal., 45(4), 197-202, 2010.
733

734 Kim, J. S.: Implications of different nitrogen input sources for primary production and carbon
735 flux estimates in coastal waters. Texas A&M University. Ph.D. Dissertation., 2018.
736

737 Kim, J. Y., Ghim, Y. S., Lee, S. B., Moon, K. C., Shim, S. G., Bae, G. N., and Yoon, S. C.:
738 Atmospheric Deposition of Nitrogen and Sulfur in the Yellow Sea Region: Significance
739 of Long-Range Transport in East Asia. Water, Air, and Soil Pollution., 205, 259-272,
740 2010.
741

742 Kim, T. W., Lee, K., Najjar, R. G., Jeong, H. D., and Jeong, H. J.: Increasing N abundance in the
743 northwestern Pacific Ocean due to atmospheric nitrogen deposition. Science., 334, 505-
744 509, 2011.
745

746 Lahiry, S.: Relationships between nutrients and dissolved oxygen concentrations on the Texas-
747 Louisiana shelf during spring-summer of 2004. Texas A & M University. MS. Thesis.,
748 2007.
749

750 Lamarque, J. F., Dentener, F., McConnell. J., Ro. C. U., Shaw. M., Vet. R., Bergmann. D.,
751 Cameron-Smith. P., Dalsoren. S., Doherty. R., Faluvegi. G., Ghan. S. J., Josse. B., Lee. Y.
752 H., MacKenzie. I. A., Plummer. D., Shindell. D. T., Skeie. R. B., Stevenson. D. S., Strode.
753 S., Zeng. G., Curran. M., Dahl-Jensen. D., Das. S., Fritzsche. D., and Nolan. M.: Multi-
754 model mean nitrogen and sulfur deposition from the Atmospheric Chemistry and Climate
755 Model Intercomparison Project (ACCMIP): evaluation of historical and projected future
756 changes. Atmospheric Chemistry and Physics., 13, 7997-8018, 2013.
757

758 Lawrence, G. B., Goolsby, D. A., Battaglin, W. A., and Stensland, G. J.: Atmospheric nitrogen in
759 the Mississippi River Basin-emissions, deposition and transport. Science of The Total
760 Environment., 248(2-3), 87-100, 2000.
761

762 Laurent, A., Fennel, K., Hu, J., and Hetland, R. D.: Simulating the effects of phosphorus
763 limitation in the Mississippi and Atchafalaya River plumes. Biogeosciences., 9, 4797-
764 4723, 2012.
765

766 Lee, J. S., Kim, K. H., Shim, J. H., Han, J. H., Choi, Y. H., and Khang, B. J.: Massive
767 sedimentation of fine sediment with organic matter and enhanced benthic-pelagic
768 coupling by an artificial dyke in semi-enclosed Chonsu Bay, Korea. Marine Pollution
769 Bulletin., 64, 153-163, 2012.
770

771 Lim, D., Kang, M. R., Jang, P. G., Kim, S. Y., Jung, H. S., Kang, Y. S., and Kang, U. S.: Water
772 Quality Characteristics Along Mid-Western Coastal Area of Korea. Ocean and Polar
773 Research., 30(4), 379-399, 2008.
774

- 775 Liu, S. M., Zhang, J., Chen, S. Z., Chen, H. T., Hong, G. H., Wei, H., and Wu, Q. M.: Inventory
776 of nutrient compounds in the Yellow Sea. *Continental Shelf Research.*, 23, 1161-1174,
777 2003.
778
- 779 Lehrter, J. C., Beddick Jr., D. L., Devereux, R., Yates, D. F., and Murrell. M. C.: Sediment-water
780 fluxes of dissolved inorganic carbon, O₂, nutrients, and N₂ from the hypoxic region of
781 the Louisiana continental shelf. *Biogeochemistry*, 109, 233–252, 2012.
782
- 783 Lohrenz, S. E., Wiesenburg, D. A., Arnone, R. A., and Chen, X. G.: What controls primary
784 production in the Gulf of Mexico? In: Sherman K, Kumpf H, Steidinger K (ed) *The Gulf*
785 *of Mexico Large Marine Ecosystem: Assessment, sustainability and management.*
786 *Blackwell Science, Malden, MA., 151-170, 1998.*
787
- 788 Lohrenz, S. E., Fahnenstiel, G. L., Redalje, D. G., Lang, G. A., Dagg, M. J., Whittedge, T. E.,
789 and Dortch, Q.: Nutrients, irradiance, and mixing as factors regulating primary
790 production in coastal waters impacted by the Mississippi River plume. *Continental Shelf*
791 *Research.*, 19, 1113-1141, 1999.
792
- 793 Luo, X. S., Tang, A. H., Shi, K., Wu, L. H., Li, W. Q., Shi, W. Q., Shi, X. K., Erisman, J. W.,
794 Zhang, F. S., and Liu, X. J.: Chinese coastal seas are facing heavy atmospheric nitrogen
795 deposition. *Environmental Research Letters.*, 9, 1-10, 2014.
796
- 797 McCarthy, M. J., Newell, S. E., Carini, S. A., and Cardner, W. S.: Denitrification dominates
798 sediment nitrogen removal and is enhanced by bottom-water hypoxia in the Northern
799 Gulf of Mexico. *Estuaries and Coasts.*, 38, 2279-2294. 2015.
800
- 801 Milliman, J. D., and Meade, R. H.: World-wide delivery of river sediment to the oceans. *The*
802 *Journal of Geology.*, 91(1), 1-21, 1983.
803
- 804 Nipper, M., Sanchez Chavez, J. A., Tunnell, Jr. J. W.: “Marsh Island,” “Calcasieu Lake,” and
805 “General Facts about the Gulf of Mexico.” *GulfBase: Resource Database for Gulf of*
806 *Mexico Research.*, 2004.
807
- 808 Nowlin, W. D. Jr., Jochens, A. E., Reid, R. O., and DiMarco, S. F.: Texas-Louisiana Shelf
809 Circulation and Transport processes Study: Synthesis Report, Volume I: Technical
810 Report. OCS Study MMS 98-0035. U.S. Dept. of the Interior, Minerals Mgmt Service,
811 Gulf of Mexico OCS Region, New Orleans, LA., 502, 1998a.
812
- 813 Nowlin, W. D. Jr., Jochens, A. E., Reid, R. O., and DiMarco, S. F.: Texas-Louisiana Shelf
814 Circulation and Transport processes Study: Synthesis Report, Volume II: Appendices.
815 OCS Study MMS 98-0036. U.S. Dept. of the Interior, Minerals Mgmt Service, Gulf of
816 Mexico OCS Region, New Orleans, LA., 288, 1998b.
817
- 818 Nunnally, C., Quigg, A., DiMarco, S. F., Chapman, P., and Rowe, G. T.: Benthic-Pelagic
819 Coupling in the Gulf of Mexico Hypoxic Area: Sedimentary enhancement of hypoxic

820 conditions and near bottom primary production. *Continental Shelf Research.*, 85, 143-152,
821 2014.

822

823 Paerl, H. W., Dennis, R. L., and Whittall, D. R.: Atmospheric Deposition of Nitrogen:
824 Implications for Nutrient Over-Enrichment of Coastal Waters. *Estuaries.*, 25(4B), 677-
825 693, 2002.

826

827 Paerl, H. W.: Controlling Eutrophication along the Freshwater-Marine Continuum: Dual Nutrient
828 (N and P) Reductions are Essential. *Estuaries and Coasts.*, 32, 593-601, 2009.

829

830 Park, M. J., Savenije, H. H. G., Cai, H., Jee, E. K., and Kim, N. H.: Progressive change of tidal
831 wave characteristics from the eastern Yellow Sea to the Asan Bay, a strongly convergent
832 bay in the west coast of Korea. *Ocean Dynamics.*, 67, 1137-1150, 2017.

833

834 Park, Y. H.: Analysis of characteristics of Dynamic Tidal Power on the west coast of Korea.
835 *Renewable and Sustainable Energy Reviews.*, 68, 461-474, 2017.

836

837 Qureshi, N. A.: The role of fecal pellets in the flux of carbon to the sea floor on a river-
838 influenced continental shelf subject to hypoxia. Louisiana State University. Ph.D.
839 Dissertation., 1995.

840

841 Quigg, A., Sylvan, J., Gustafson, A., Fisher, T., Oliver, R., Tozzi, S., and Ammerman, J.: Going
842 west: nutrient limitation of primary production in the northern Gulf of Mexico and the
843 importance of the Atchafalaya River. *Aquatic Geochemistry.*, 17, 519-544, 2011.

844

845 Rabalais, N. N., and Smith, L. E.: The effects of bottom water hypoxia on benthic communities
846 of the southeastern Louisiana continental shelf. New Orleans, Louisiana, U.S. Minerals
847 Management Service, Gulf of Mexico OCS Region., 105, 1995.

848

849 Rabalais, N. N., and Turner, R. E.: Hypoxia in the Northern Gulf of Mexico: Description, causes
850 and change, pp. 1–36. In N. N. Rabalais and R. E. Turner (eds.), *Coastal Hypoxia:
851 Consequences for Living Resources and Ecosystems.* Coastal and Estuarine Studies., 58,
852 2001.

853

854 Rabalais, N. N., Turner, R. E., and Scavia, D.: Beyond science into policy: Gulf of Mexico
855 hypoxia and the Mississippi river. *Bioscience.* Vol.52(2). pp.129-142, 2002.

856

857 Rabalais, N. N., Turner, R. E., Sen Gupta, B. K., Boesch, D. F., Chapman, P., and Murrell, M. C.:
858 Hypoxia in the northern Gulf of Mexico: Does the science support the plan to reduce,
859 mitigate, and control hypoxia? *Estuaries Coastal.*, 30, 753-772, 2007.

860

861 Rabalais, N. N., Turner, R. E., Justic, D., Diaz, R. J.: Global change and eutrophication of coastal
862 waters. *ICES. Journal of Marine Science.*, 66, 1528–1537, 2009.

863

864 Ramesh. R., Chen. Z., Cummins. V., Day. J., D’Elia. C., Dennison. B., Forbes. D. L., Glaeser. B.,
865 Claser. M., Clavovic. B., Kremer. H., Lange. M., Larsen. J. N., Tissier. M. Le., Newton.

866 A., Pelling, M., Purvaja, R., and Wolanski, E.: Land-ocean interactions in the coastal
867 zone: past, present & future, *Anthropocene.*, 12, 85-98, 2015.

868

869 Redalje, D. G., Lohrenz, S. E., and Fahnenstiel, G. L.: The relationship between primary
870 production and the vertical export of particulate organic matter in a river impacted coastal
871 ecosystem. *Estuaries.*, 17, 829-838, 1994.

872

873 Robertson, D. M., and Saad, D. A.: SPARROW Models Used to Understand Nutrient Sources in
874 the Mississippi/Atchafalaya River Basin. *Journal of Environmental Quality.*, 42, 1422-
875 1440, 2014.

876

877 Rowe, G. T., and Chapman, P.: Continental Shelf Hypoxia: some nagging questions. *Gulf
878 Mexico Science.*, 20, 153-160, 2002.

879

880 Rowe, G. T., Kaegi, M. E. C., Morse, J. W., Boland, G. S., and Briones, E. G. E.: Sediment
881 community metabolism associated with continental shelf hypoxia, northern Gulf of
882 Mexico. *Estuaries.*, 25(6), 1097–1106, 2002.

883

884 Scavia, D., Justic, D., and Bierman, V. J.: Reducing Hypoxia in the Gulf of Mexico: Advice
885 from Three Models. *Estuaries.*, 27(3), 419-425. 2004.

886

887 Scavia, D., Evans, M. A., and Obenour, D. R.: A scenario and forecast model for Gulf of Mexico
888 hypoxic area and volume. *Environmental Science and Technology.*, 47, 10423-10428,
889 2013.

890

891 Shou, W., Zong, H., Ding, P., and Hou, L.: A modelling approach to assess the effects of
892 atmospheric nitrogen deposition on the marine ecosystem in the Bohai Sea, China.
893 *Estuarine, Coastal and Shelf Science.*, 208, 36-48, 2018.

894

895 Sigman, D. M., and Hain, M. P.: The Biological Productivity of the Ocean. *Nature Education.*, 3,
896 1-16, 2012.

897

898 Son, S. H., Campbell, J. W., Dowell, M., Yoo, S. J., and Noh, J.: Primary production in the
899 Yellow Sea determined by ocean color remote sensing. *Marine Ecology Progress Series.*,
900 303, 91-103, 2005.

901

902 Sylvan, J. B., Dortch, Q., Nelson, D. M., Maier Brown, A. F., Morrison, W., Ammerman, J. W.:
903 Phosphorus limits phytoplankton growth on the Louisiana shelf during the period of
904 hypoxia formation. *Environmental Science and Technology.*, 40(24), 7548– 7553, 2006.

905

906 Testa, J. M., Kemp, W. M., Boynton, W. R., and Hagy, J. D: Long-term changes in water quality
907 and productivity in the Patuxent river estuary: 1985 to 2003. *Estuaries and Coasts.*, 31,
908 1021-1037, 2008.

909

910 Thornton, D. C. O., Dong, L. F., Underwood, G. J. C., and Nedwell, D. B.: Sediment-water
911 inorganic nutrient exchange and nitrogen budgets in the Colne Estuary, UK. *Marine*
912 *Ecology Progress Series.*, 337, 63-77, 2007.
913

914 Turner, R. E., and Rabalais, N. N.: Changes in the Mississippi River nutrient supply and offshore
915 silicate-based phytoplankton community responses. In Dyer, K.R and R. J Orth(eds.).
916 *Changes in Fluxes in Estuaries: Implications from Science to management Proceedings*
917 *of ECSA22/ERF Symposium. International Symposium Series. Olsen and Olsen.*
918 *Gredensborg. Denmark.,147-150, 1994.*
919

920 Turner, R. E., Rabalais, N. N., and Justic, D.: Predicting summer hypoxia in the northern Gulf of
921 Mexico: riverine N, P and Si loading. *Marine Pollution Bulletin.*, 51, 139-148, 2006.
922

923 Turner, R. E., Rabalais, N. N., and Justic, D.: Gulf of Mexico Hypoxia: Alternate States and a
924 Legacy. *Environmental Science and Technol.*, 42, 2323-2327, 2008.
925

926 Turner, R. E., and Rabalais, N. N.: Nitrogen and phosphorus phytoplankton growth limitation in
927 the northern Gulf of Mexico. *Aquatic microbial ecology.*, 68, 159–169, 2013.
928

929 Wade, T. L., and Sweet, S. T.: Final Report Coastal Bend Bays and Estuaries Program (CBBEP):
930 Atmospheric Deposition Study., 48pp, 2008.
931

932 Wang, H., Dai, M., Liu, J., Kao, S. J., Zhang, C., Cai, W. J., Wang, G., Qian, W., Zhao, M., and
933 Sun, Z.: Eutrophication-Driven Hypoxia in the East China Sea off the Changjiang
934 Estuary. *Environmental Science & Technology.*, 50, 2255-2263, 2016.
935

936 Yang, J. S., and Ahn, T. Y.: The analysis of the correlation between groundwater level and the
937 moving average of precipitation in Kuem river watershed. *The Journal of Engineering*
938 *Geology.*, 18, 1-6, 2008.
939

940 Zhao, Y., Zhang, L., Pan, Y., Wang, Y., Paulot, F., and Henze, D. K.: Atmospheric nitrogen
941 deposition to the northwestern Pacific: seasonal variation and source attribution. *Atmos.*
942 *Chem. Phys.*, 15, 10905-10924, 2015.
943

944 **List of Figures**

- 945 Figure 1. Study sites and sampling areas in the GOM and Korea. Figure (a) shows the sampling
946 area within the northern GOM, and (b) shows station positions from March 2005. Note
947 that MCH project data are widely distributed across the region. Figure (c) shows the
948 sampling area off the west coast of Korea and (d) shows all of the station positions.
949
- 950 Figure 2. The Rowe and Chapman three zone hypothesis, which described the physical and
951 biochemical processes that initiate and sustain hypoxia on the Texas-Louisiana Shelf,
952 [Rowe and Chapman, 2002]. *Reprinted with permission of Gulf of Mexico Science.*
953
- 954 Figure 3. (a) Input (blue) and output (red) sources for each 0.25° box in the GOM and CSK (see
955 text for details); (b) Area of each sub-region (red) and boxes affected by direct riverine
956 input (blue) in the GOM. Export N (Mixing) represents the advective transport term.
957 The processes of biogeochemical and transport processes of both regions are the same
958 and each in/out put factor is the same in the GOM and CSK. Note that transfer
959 between boxes occurs in both directions alongshore and onshore/offshore and is not a
960 one-dimensional process as suggested in the diagram.
961
- 962 Figure 4. Mean ocean current velocities (a) and standard deviations (b) for biweekly periods
963 from August 1993 through December 1994 based on data from LATEX project.
964 Positive values of U show eastward flow; positive values of V show northward flow.
965
- 966 Figure 5. Extent of the three zones defined by RC02 based on the mean concentration of nutrient
967 (DIN) at each station during the MCH M4 cruise in March 2005, showing their
968 correspondence to the three sub-regions used in the box model. Red, grey and blue
969 stations correspond to sub-regions A (near the Mississippi River), B (between the
970 Mississippi and Atchafalaya), and C (near the Atchafalaya) respectively.
971
- 972 Figure 6a. Areal distributions of the three zones using data from above the pycnocline, based on
973 N mass balance model results. Colors and numbers represent boxes found in each of
974 the three zones in terms of potential productivity (Unit: $\text{gC m}^{-2} \text{day}^{-1}$).
975
- 976 Figure 6b. As for 6a, using data from below the pycnocline.
977
- 978 Figure 7a. The distribution of the three zones off Mid-western Korea (CSK) above the
979 pycnocline based on the RC02 hypothesis applied to the N mass balance model.
980 Colors and numbers represent boxes found in each of the three zones in terms of
981 potential productivity (Unit: $\text{gC m}^{-2} \text{day}^{-1}$).
982
- 983 Figure 7b. As for 7a, using data from below the pycnocline
984
- 985 Figure 8. Distribution of the three zones during cruises MCH M1-M3 based on salinity data
986 (Lahiry, 2007). Areas shaded in three colors represent the brown, green and blue zones
987 respectively.
988
- 989 Figure 9. DIN against DIP during sampling periods in the GOM and CSK. Nearly all samples

990 had an N:P ratio of < 16 , which indicated potential N-limited condition. At a few
991 points near the brown zone the ratio was between 16 -18; this is where light-limitation
992 is expected according to RC02.
993

994 **List of Tables**

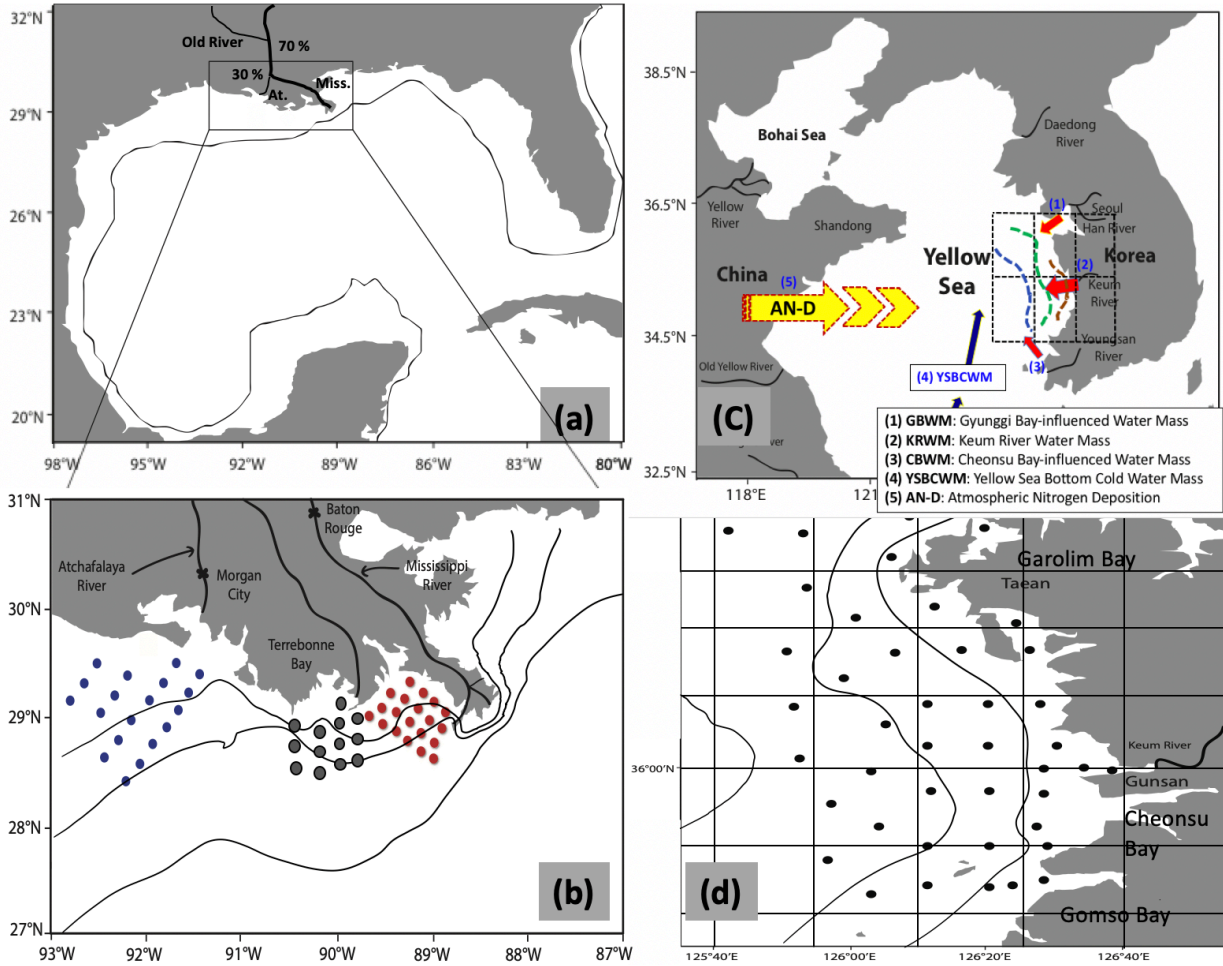
995 Table 1. Sampling dates for data from Gulf of Mexico projects and the coastal sea of Korea.
996 Winter data are listed for the Gulf of Mexico cruises.

997
998 Table 2. Atmospheric Nitrogen Deposition (AN-D) in the USA and in the Yellow Sea.
999

1000 Table 3. Definitions and values used in N-mass balance model to calculate DIN removal by
1001 biological production. (a) Each one quarter degree box; (b) Wade and Sweet 2008 for
1002 GOM region; (c) McCarthy et al., 2015 (d) Lee et al., 2012; (e) McCarthy et al., 2015;
1003 (f) Qureshi 1995. * F_{Atmo}^{DIN} of CSK region is used as mean values of Asia data in Table 2,
1004 which is initially 5 times higher than that of GOM ($1.4 \times 10^5 \text{ mol day}^{-1}$). ** The unit of
1005 F_{Sink}^{DIN} was converted to mol day^{-1} from the unit of original data ($\text{gN m}^{-2} \text{ day}^{-1}$) with area
1006 of box ($0.25 \text{ m} \times 0.25 \text{ m}$) and molar mass of N (14 g mol^{-1}). All unit were converted
1007 to mol day^{-1} multiplied by area of box ($0.25 \text{ m} \times 0.25 \text{ m}$).
1008

1009 Table 4. Simulation results for selected model scenarios based on MCH M1 (April 5-7, 2004), as
1010 described in the text. Biological production is calculated using our N-mass balance
1011 model, while oxygen demand is calculated by the Redfield stoichiometry ratio (C: O₂ =
1012 106: 138) (Unit: $\text{gC m}^{-2} \text{ day}^{-1}$).
1013

1014 Table 5. Simulation results for selected model scenarios based on CSK (February 2008) data, as
1015 described in the text. Biological production is calculated using our N-mass balance
1016 model, while oxygen demand is calculated by the Redfield stoichiometry ratio (C: O₂ =
1017 106: 138) (Unit: $\text{gC m}^{-2} \text{ day}^{-1}$).
1018



1019

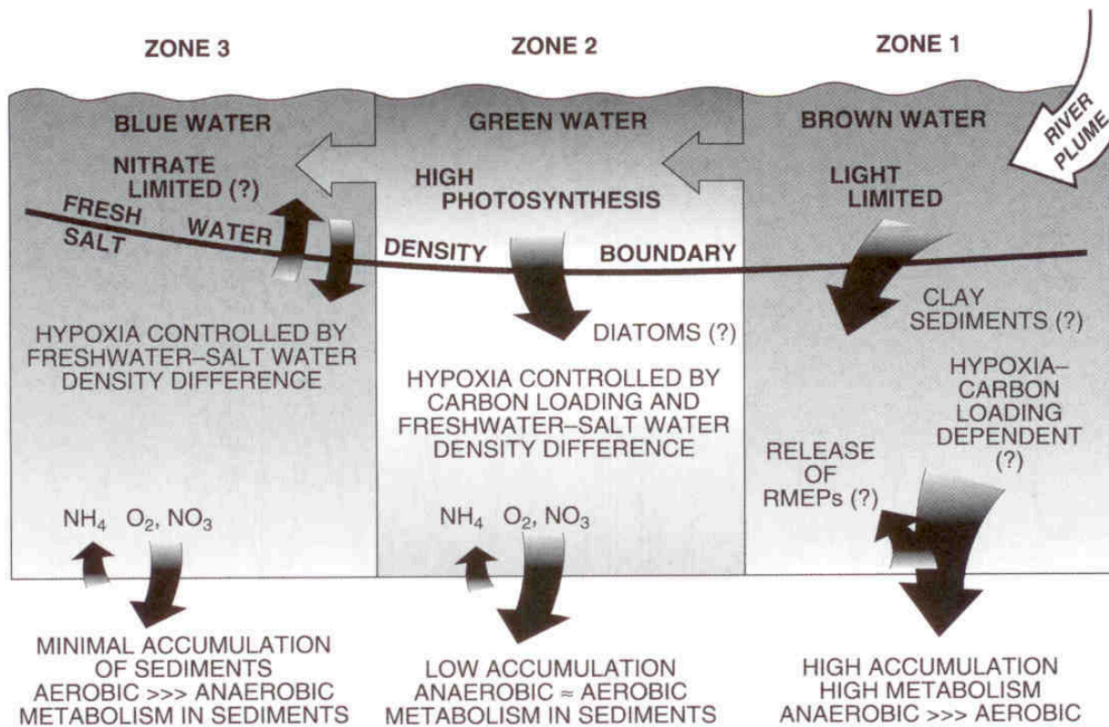
1020

1021

1022

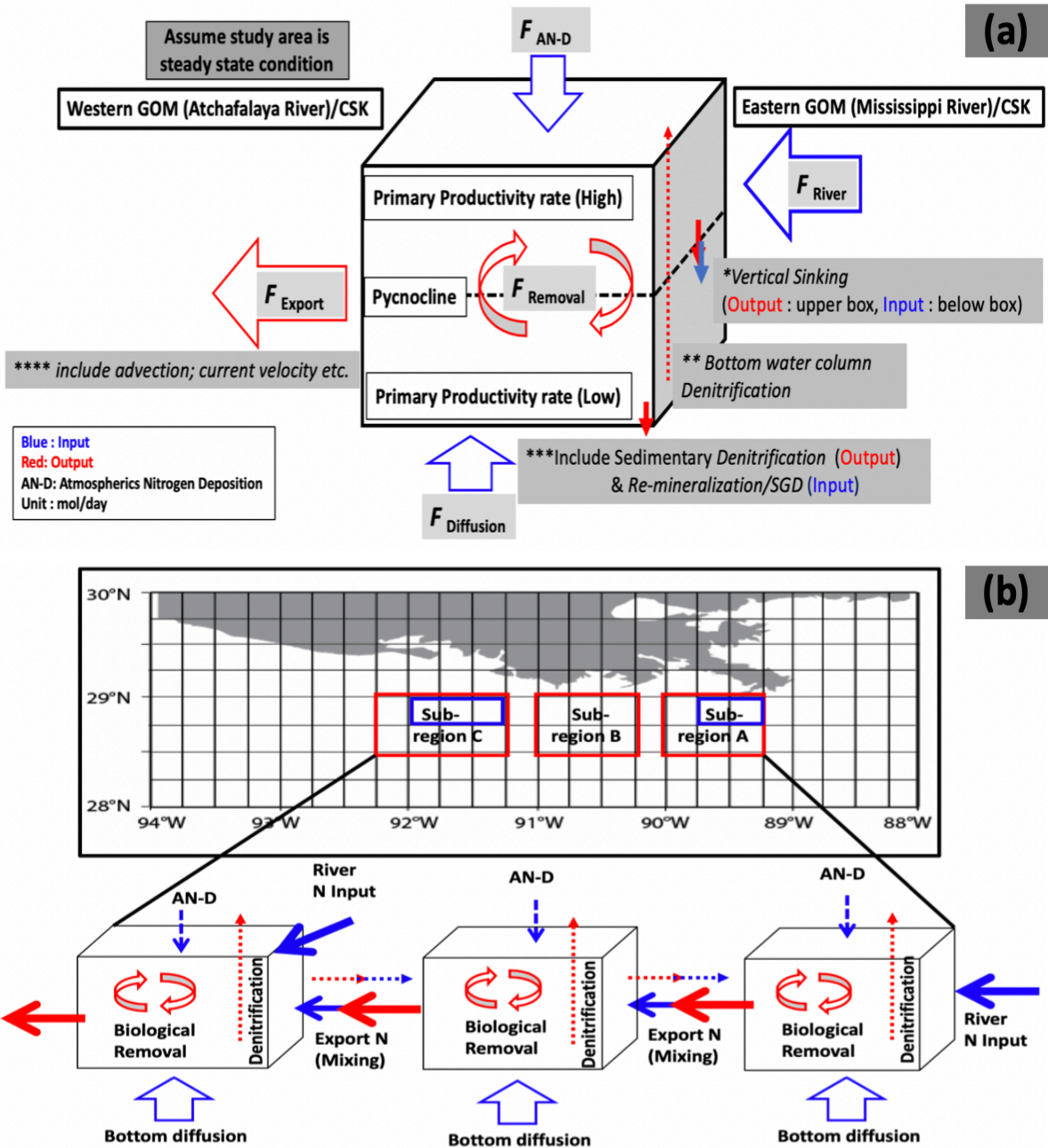
1023

Figure 1. Study sites and sampling areas in the GOM and Korea. Figure (a) shows the sampling area within the northern GOM, and (b) shows station positions from March 2005. Note that MCH project data are widely distributed across the region. Figure (c) shows the sampling area off the west coast of Korea and (d) shows all of the station positions.



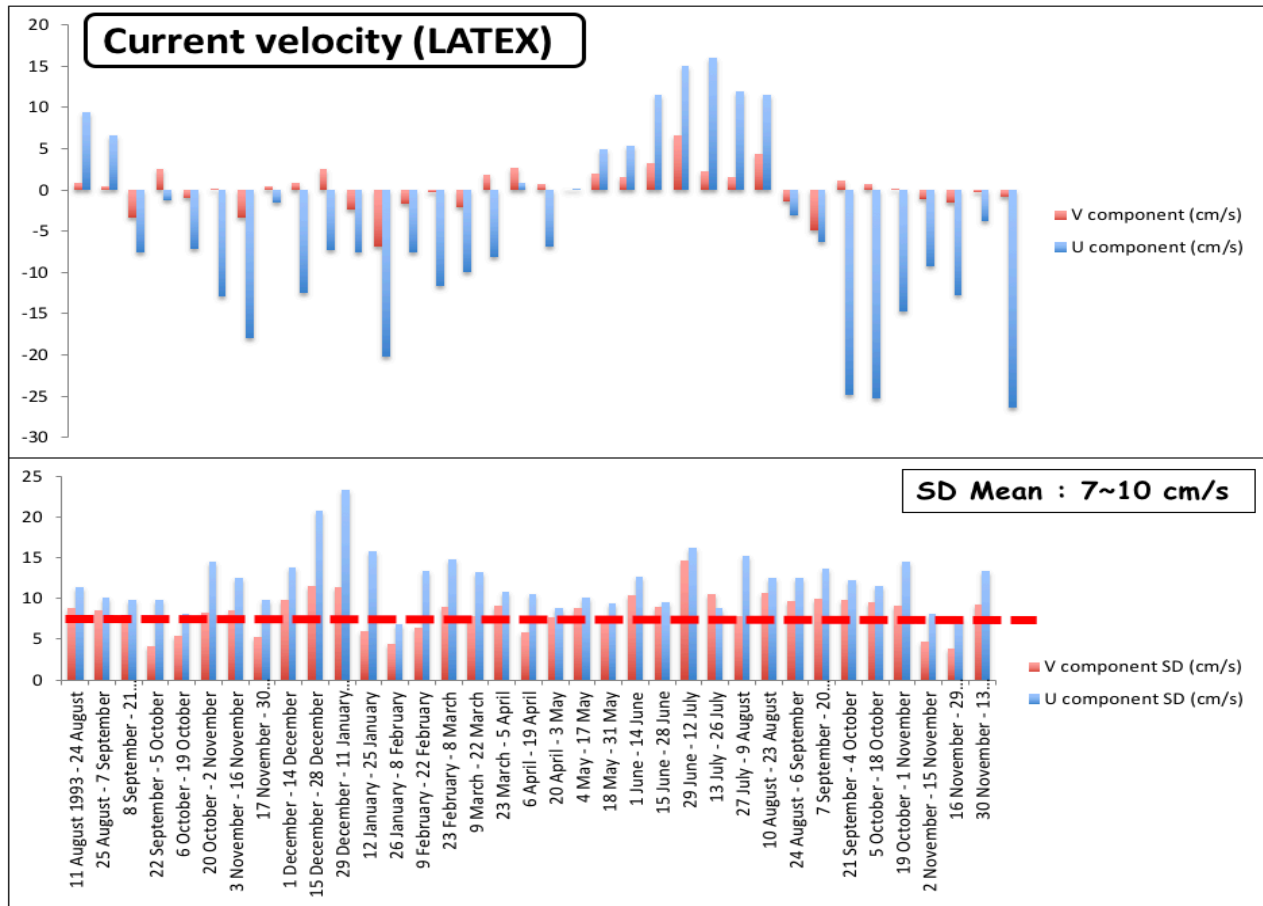
1024

1025 **Figure 2.** The Rowe and Chapman three zone hypothesis, which described the physical and
 1026 biochemical processes that initiate and sustain hypoxia on the Texas-Louisiana Shelf, [Rowe and
 1027 Chapman, 2002]. *Reprinted with permission of Gulf of Mexico Science.*



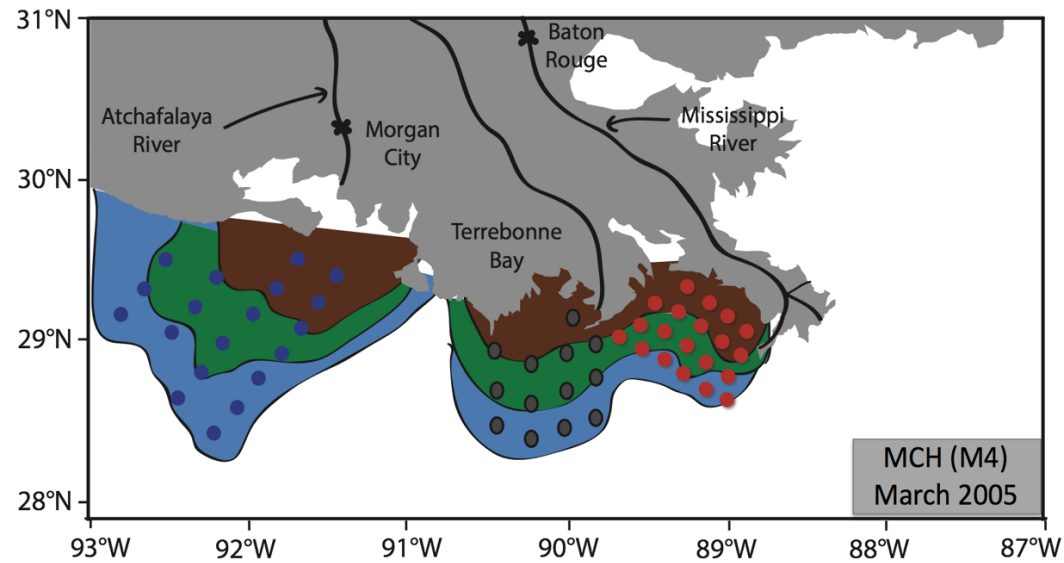
1028

1029 **Figure 3.** (a) Input (blue) and output (red) sources for each 0.25° box (see text for details); (b)
 1030 Area of each sub-region (red) and boxes affected by direct riverine input (blue). Export N
 1031 (Mixing) represents the advective transport term. The processes of biogeochemical and
 1032 transport processes of both regions are the same and each in/out put factor is the same in the
 1033 GOM and CSK. Note that transfer between boxes occurs in both directions alongshore and
 1034 onshore/offshore and is not a one-dimensional process as suggested in the diagram.
 1035



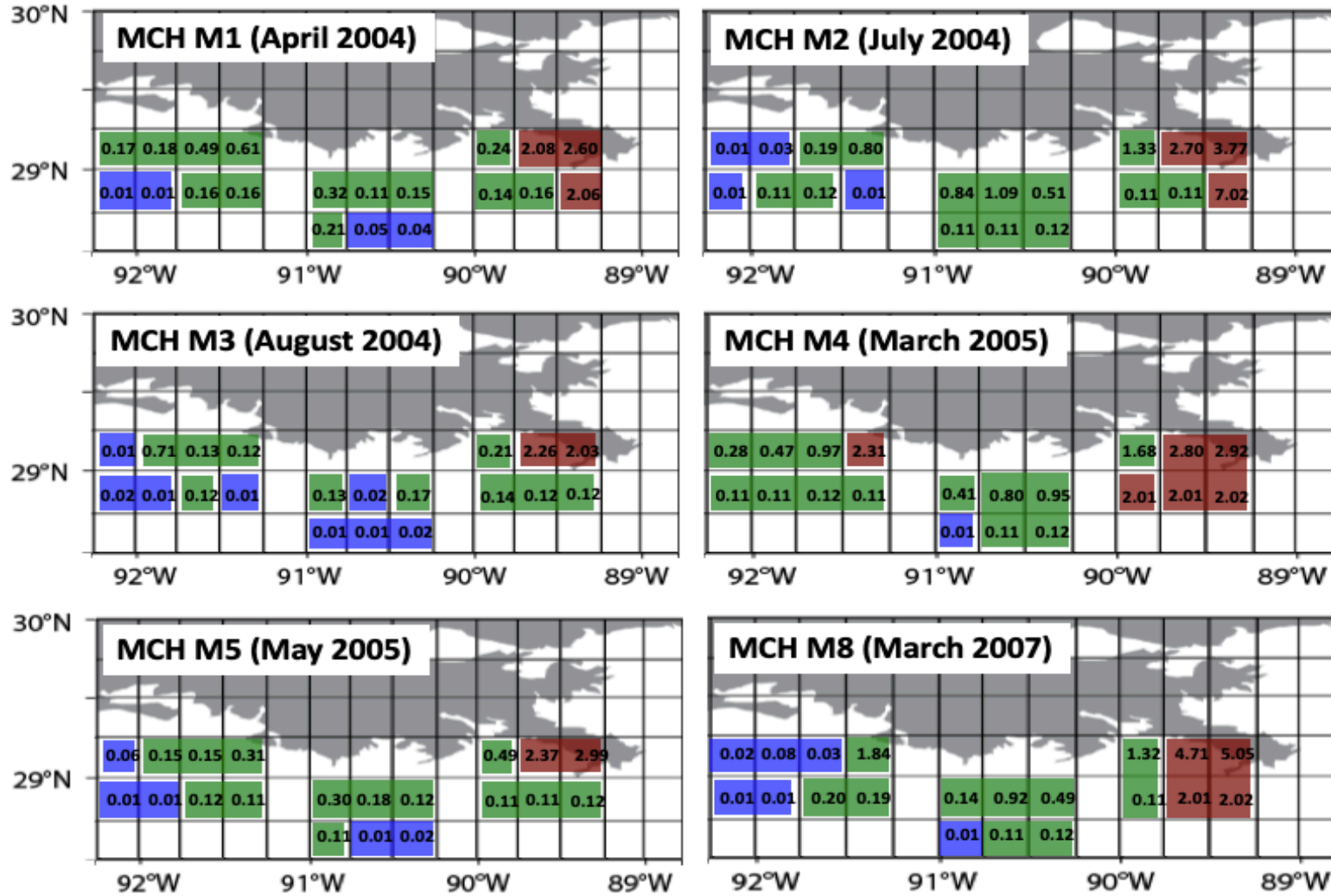
1036
 1037
 1038
 1039

Figure 4. Mean ocean current velocities (a) and standard deviations (b) for biweekly periods from August 1993 through December 1994 based on data from LATEX project. Positive values of U show eastward flow; positive values of V show northward flow.



1040

1041 **Figure 5.** Extent of the three zones defined by RC02 based on the mean concentration of nutrient (DIN) at each station during the MCH M4
 1042 cruise in March 2005, showing their correspondence to the three sub-regions used in the box model. Red, grey and blue stations correspond to
 1043 sub-regions A (near the Mississippi River), B (between the Mississippi and Atchafalaya), and C (near the Atchafalaya) respectively.
 1044

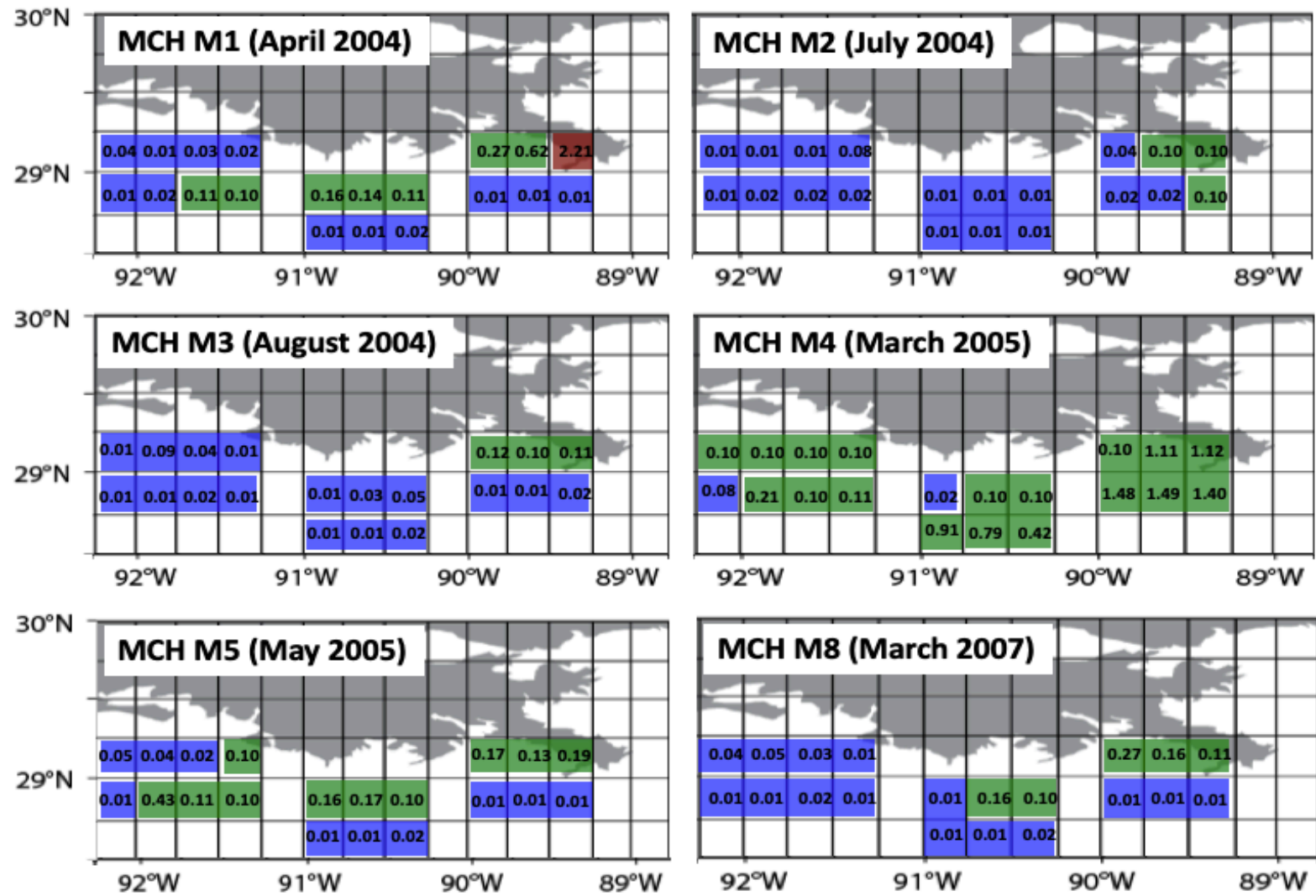


1045

1046

1047

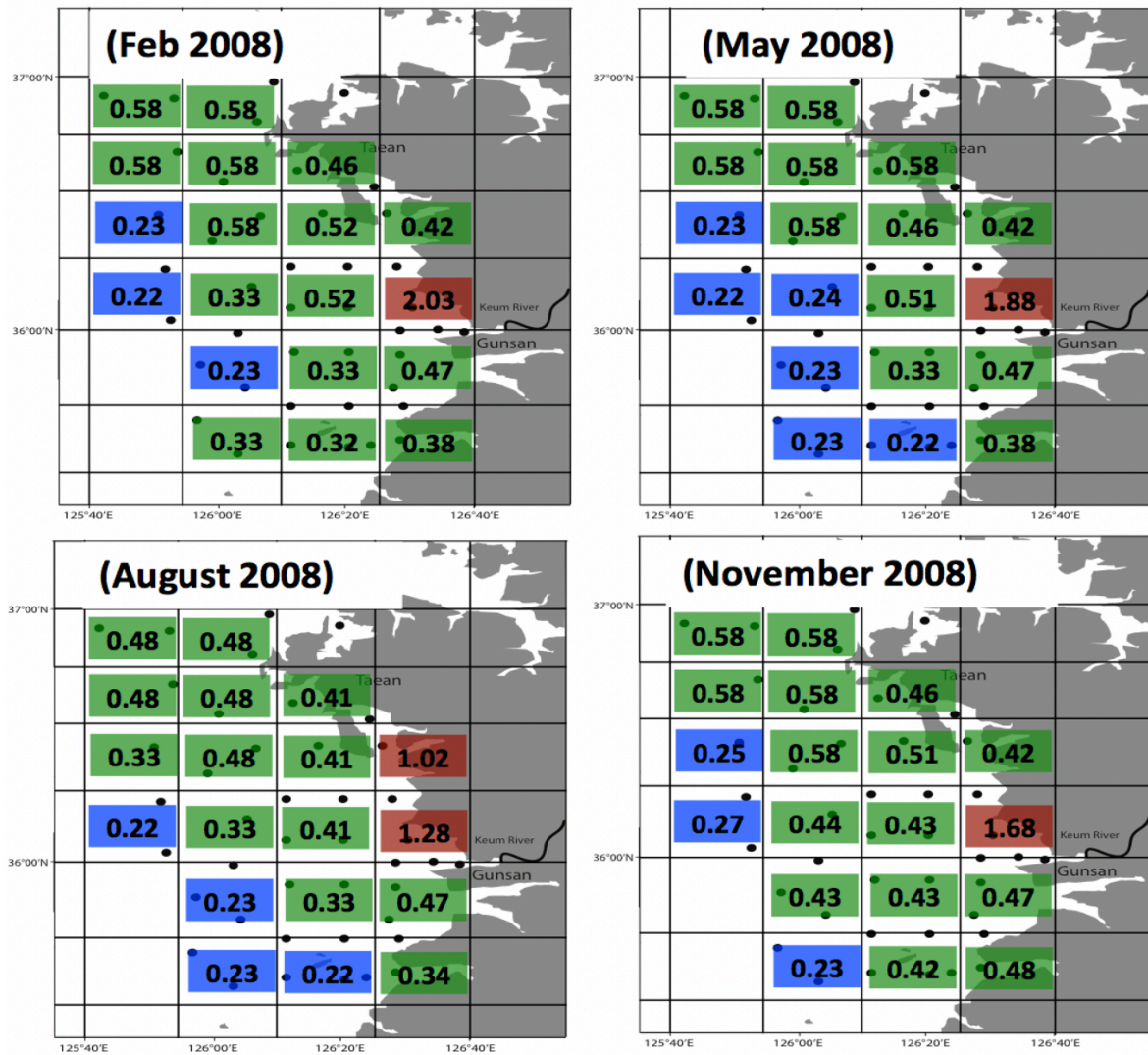
Figure 6a. Areal distributions of the three zones using data from above the pycnocline, based on N-mass balance model results. Colors and numbers represent boxes found in each of the three zones in terms of potential productivity (Unit: $\text{gC m}^{-2} \text{day}^{-1}$).



1048

1049 **Figure 6b.** As for 6a, using data from below the pycnocline.

CSK (Above pycnocline)

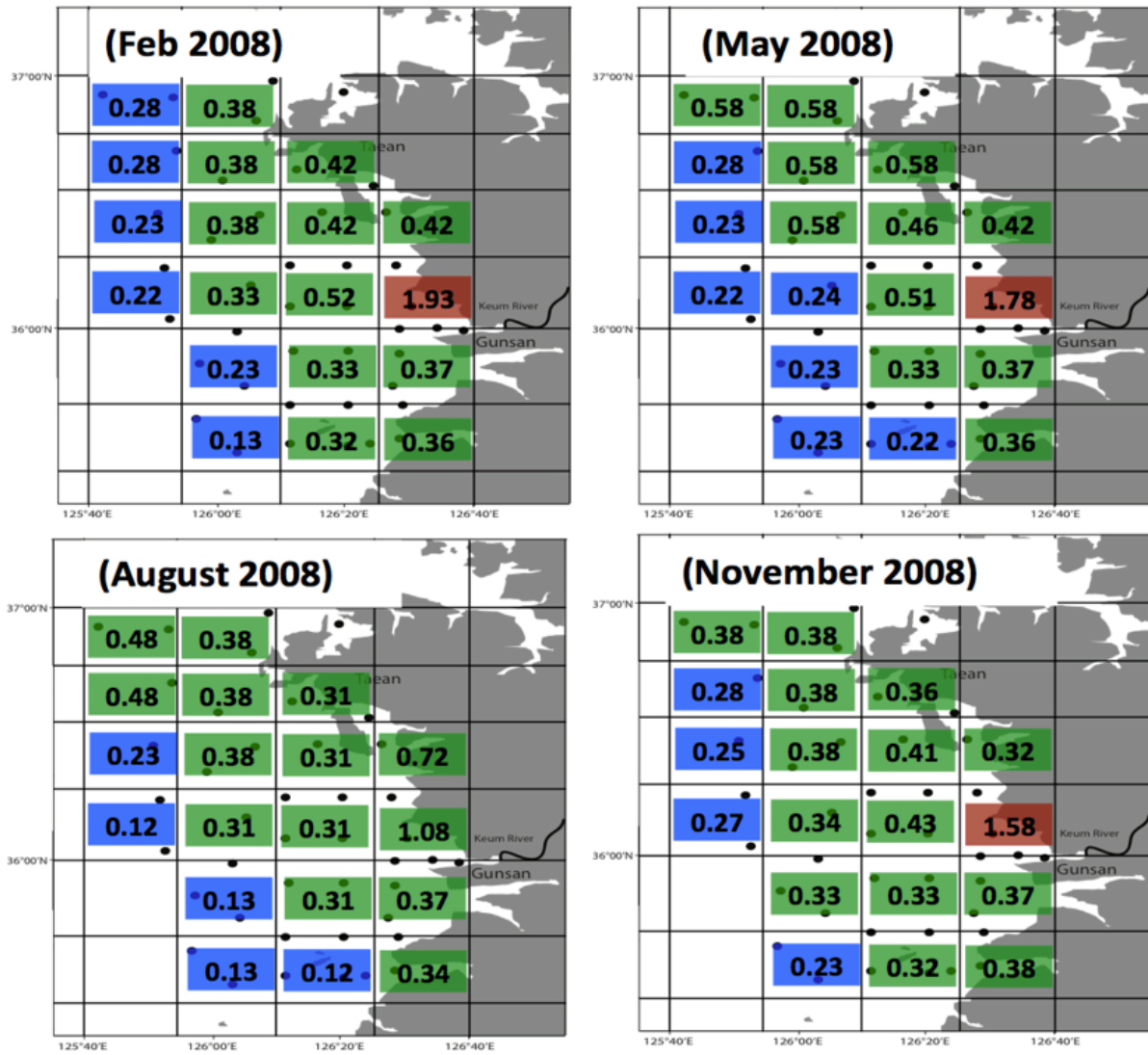


1050

1051 **Figure 7a.** The distribution of the three zones off Mid-western Korea (CSK) above the
 1052 pycnocline based on the RC02 hypothesis applied to the N mass balance model. Colors and
 1053 numbers represent boxes found in each of the three zones in terms of potential productivity
 1054 (Unit: gC m⁻² day⁻¹).

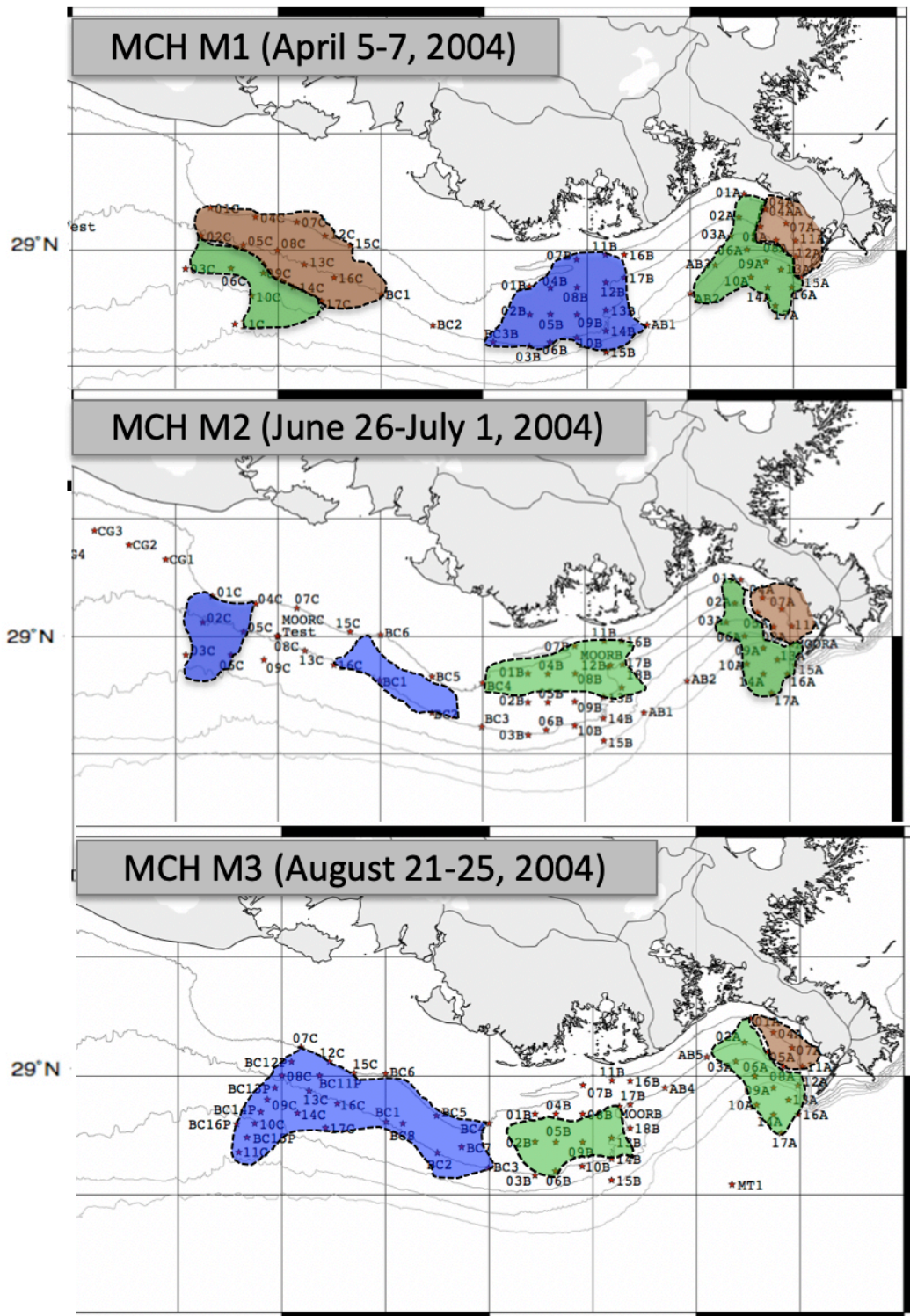
1055

CSK (Below pycnocline)



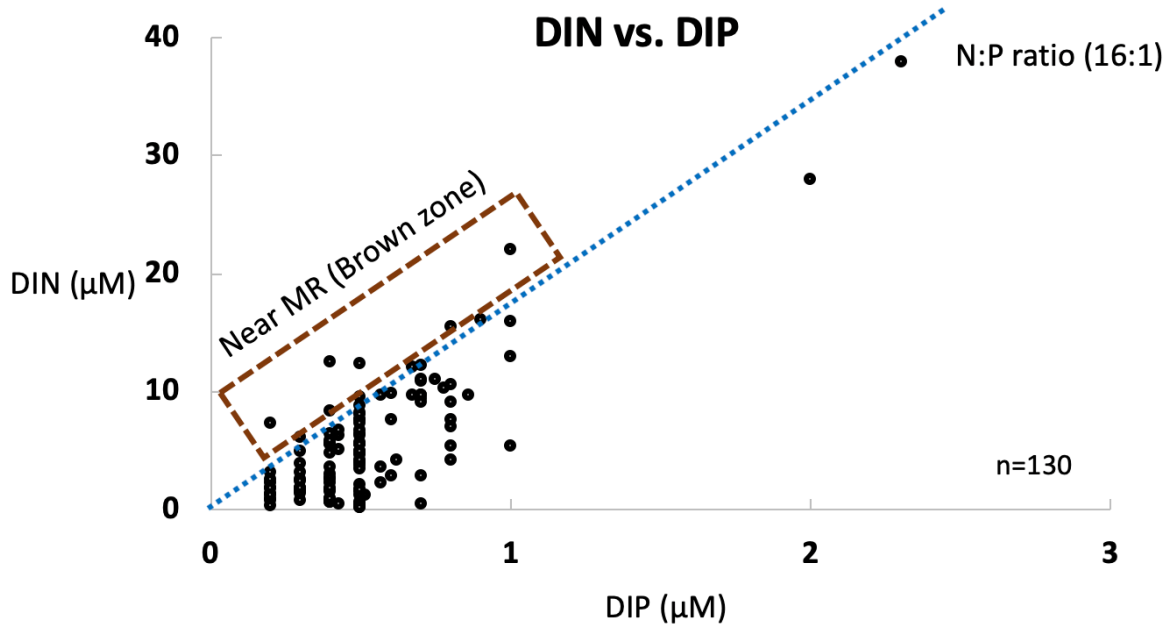
1056

1057 **Figure 7b.** As for 7a, using data from below the pycnocline.



1058
 1059
 1060
 1061
 1062

Figure 8. Distribution of the three zones during cruises MCH M1-M3 based on salinity data (Lahiry, 2007). Areas shaded in three colors represent the brown, green and blue zones respectively.



1063
 1064
 1065
 1066
 1067
 1068

Figure 9. DIN against DIP during sampling periods in the GOM and CSK. Nearly all samples had an N:P ratio of < 16, which indicated potential N-limited condition. At a few points near the brown zone the ratio was between 16 -18; this is where light-limitation is expected according to RC02.

1069 **Table 1.** Sampling dates for data from Gulf of Mexico projects and the coastal sea of Korea.
 1070 Winter data are listed for the Gulf of Mexico cruises.

Study area	Date	Cruise number
Gulf of Mexico MCH	April 5~7, 2004	MCH M1
	June 26~July 1, 2004	MCH M2
	August 21~25, 2004	MCH M3
	March 23~27, 2005	MCH M4
	May 20~26, 2005	MCH M5
	March 23~29, 2007	MCH M8
Korea CSK	Feb, May, Aug, Nov (2008)	

1071

1072

1073

1074

Table 2. Atmospheric Nitrogen Deposition (AN-D) in the USA and in the Yellow Sea.

Watersheds	AN-D (Kg/ha/year)	References
Casco Bay, ME	1.5	Castro and Driscoll. 2002
Merrimack River, MA	1.2 ~ 4.0	Alexander et al. 2000
Long Island Sound, CT	1.8	Castro and Driscoll. 2002
Delaware Bay, DE	2.2 ~ 4.4	Castro and Driscoll. 2002 Goolsby. 2000
Chesapeake Bay	1.4 ~ 17.4	Alexander et al. 2000 Castro, M. S et al. 2000 Castro and Driscoll. 2002 Goolsby. 2000
Gulf of Mexico	10.0 ~ 11.5	Wade and Sweet. 2008
Bohai Sea	64.2 ~ 142.5	Shou et al. 2018
Yellow Sea (China on the west side)	16.1 ~ 18.4	Zhao et al. 2015
	29.9 ~ 32.8	Luo et al. 2014
	38.1 ~ 92.4	Shou et al. 2018
Yellow Sea (Korea on the east side)	15.0 ~ 58.2	Kim (JY) et al. 2010

1075

1076

1077 **Table 3.** Definitions and values used in N-mass balance model to calculate DIN removal by biological production. (a) Each one quarter degree
 1078 box; (b) Wade and Sweet 2008 for GOM region; (c) McCarthy et al., 2015 (d) Lee et al., 2012; (e) McCarthy et al., 2015; (f) Qureshi 1995.
 1079 * F_{Atmo}^{DIN} of CSK region is used as mean values of Asia data in Table 2, which is initially 5 times higher than that of GOM ($1.4 \times 10^5 \text{ mol day}^{-1}$).
 1080 ** The unit of F_{Sink}^{DIN} was converted to mol day^{-1} from the unit of original data ($\text{gN m}^{-2} \text{ day}^{-1}$) with area of box (0.25 m x 0.25 m) and molar
 1081 mass of N (14 g mol^{-1}). All unit were converted to mol day^{-1} multiplied by area of box (0.25 m x 0.25 m).

Unit	Definitions	Value
A_{Bott} (m^2)	Area of box	$6.2 \times 10^8 \text{ m}^2$ (a)
C_{Box}^{DIN} (μM)	DIN concentration in each area (box)	
V_S (m^3)	Water volume of box	$A_{Bott} \times \text{Pycnocline depth}$
C_{EX}^{DIN} (mmol m^{-3})	Different concentration between each box $C_{EX} = (C_{On} - C_{Off})$ or $(C_{East} - C_{West})$ for DIN	
λ_{Mix} (day^{-1})	Mixing rate of each box to box (A reciprocal of the water residence time)	
F_{River} (day^{-1})	River discharge	
F_{River}^{DIN} (mol day^{-1})	DIN flux from each river discharge	
F_{Atmo}^{DIN} (mol day^{-1})	Diffusive flux from Atmospheric deposition (Bulk N deposition rate x A_{Bott} ($A_{\text{surface of ocean}}$) for DIN)	$1.4 \times 10^5 \text{ mol day}^{-1}$ * (b)
F_{Bott}^{DIN} (mol day^{-1})	Benthic flux from the bottom sediments (Net DIN release considered regeneration, groundwater inputs, and uptake of NO_2/NO_3)	$1.2 \text{ mmol N m}^{-2} \text{ day}^{-1}$ (c) $6.2 \text{ mmol N m}^{-2} \text{ day}^{-1}$ (d)
F_{Export}^{DIN} (mol day^{-1})	An advection term which calculated from the current velocity	
F_{Deni}^{DIN} (mol day^{-1})	Denitrification in the water column	$2.1 \text{ mmol N m}^{-2} \text{ day}^{-1}$ (e)
F_{Sink}^{DIN} (mol day^{-1})	Vertical sinking of DIN flux from sediment trap data	$0.1 \sim 1 \text{ gN m}^{-2} \text{ day}^{-1}$ ** (f)
$F_{Removal}^{DIN}$ (day^{-1})	Removal by biological production (Assuming that the other removal factors are negligible above the pycnocline layer)	

1082 **Table 4.** Simulation results for selected model scenarios based on MCH M1 (April 5-7, 2004).
 1083 Biological production is calculated by our N-mass balance model. Oxygen demand is
 1084 calculated by Redfield stoichiometry ratio (C: O₂ = 106: 138) (Unit: gC m⁻² day⁻¹).

1085

	F_{River}	$F_{\text{AN-D}}$	$F_{\text{Bott/SGD}}$	Biological production	Oxygen demand
Nominal Value	1.4 x 10 ⁷ (~98 %)	1.4 x 10 ⁵ (~1 %)	1.4 x 10 ⁵ (~1 %)	Base line	
Scenario 1	5.6 x 10 ⁶ (~93 %)	2.8 x 10 ⁵ (~5%)	1.4 x 10 ⁵ (~2%)	~45% decreased	~58% decreased
Scenario 2	9.8 x 10 ⁶ (~96 %)	2.8 x 10 ⁵ (~3%)	1.4 x 10 ⁵ (~1%)	~22% decreased	~28% decreased
Scenario 3	1.7 x 10 ⁷ (~97 %)	2.8 x 10 ⁵ (~2%)	1.4 x 10 ⁵ (~1%)	~17% increased	~21% increased

1086 **Table 5.** Simulation results for selected model scenarios based on CSK (February 2008)
 1087 data. Biological production is calculated by our N-mass balance model. Oxygen
 1088 demand is calculated by the Redfield stoichiometry ratio (C: O₂ = 106: 138) (Unit: gC m-2
 1089 day-1).
 1090

	F_{River}	$F_{\text{AN-D}}$	$F_{\text{Bott/SGD}}$	Biological production	Oxygen demand
Nominal Value	1.9 x 10 ⁶ (~60%)	6.0 x 10 ⁵ (~20%)	6.0 x 10 ⁵ (~20%)	Base line	
Scenario 1	7.2 x 10 ⁵ (~29%)	1.2 x 10 ⁶ (~47%)	6.0 x 10 ⁵ (~24%)	~13% decreased	~16% decreased
Scenario 2	1.3 x 10 ⁶ (~41%)	1.2 x 10 ⁶ (~39%)	6.0 x 10 ⁵ (~20%)	~2% decreased	~2% decreased
Scenario 3	2.2 x 10 ⁶ (~55%)	1.2 x 10 ⁶ (~30%)	6.0 x 10 ⁵ (~15%)	~25% increased	~32% increased

1091